Core Dynamics of the MJO

JI-EUN KIM[a,b] AND CHIDONG ZHANG[c]

[a] *Center for Climate Physics, Institute for Basic Science, Busan, South Korea*
[b] *Pusan National University, Busan, South Korea*
[c] *NOAA/Pacific Marine Environmental Laboratory, Seattle, Washington*

(Manuscript received 30 June 2020, in final form 22 September 2020)

ABSTRACT: The Madden–Julian oscillation (MJO) is a large-scale eastward-moving system that dominates tropical subseasonal perturbations with far-reaching impacts on global weather–climate. For nearly a half century since its discovery, there has not been a consensus on the most fundamental dynamics of the MJO, despite intensive studies with a number of theories proposed. In this study, using a simple analytical approach, we found a solution to the linear equatorial shallow-water equations with momentum damping that resembles a harmonic oscillator. This solution exhibits the key characteristics of the observed MJO: its intraseasonal periodicity at the planetary scale and eastward propagation. In contrast to theories that interpret the MJO as a new mode of variability emerging from the evolution in moisture, our solution emphasizes that the core of the MJO resides in the dynamics without explicit fluctuations in moisture. Moisture still plays a role in supplying energy to the core dynamics of the MJO, and determining the value of the equivalent depth required by the theory. The energy source may come from stochastic forcing in the tropics or from the extratropics. The scale selection for the MJO comes from scale-dependent responses to scale-independent Rayleigh damping. We also demonstrate that the MJO solution introduced here reproduces the observed swallowtail structure and the phase relation between zonal wind and geopotential of the MJO, and the continuum nature of the transition between the MJO and Kelvin waves. Roles of feedback mechanisms in the MJO are also discussed using the same simple mathematical framework.

KEYWORDS: Atmospheric circulation; Convection; Dynamics; Madden-Julian oscillation; Waves, atmospheric; Intraseasonal variability

1. Introduction

The tropical Indian and Pacific Oceans experience huge fluctuations in rainfall accompanied by strong easterly and westerly wind anomalies at the lower and upper troposphere on intraseasonal time scales (30–60 days) and the planetary zonal scale (zonal wavenumber $k = 1$). These fluctuations in rainfall normally start over the Indian Ocean and move eastward slowly ($\sim 5\,\mathrm{m\,s^{-1}}$) into the Pacific. Such fluctuations were first scientifically documented by Madden and Julian (1971, 1972). They are now known as the Madden–Julian oscillation (MJO).

The MJO provides a major source of predictability at intraseasonal scales (National Academies of Sciences, Engineering, and Medicine 2016; Waliser et al. 2003). It has broad impacts on global weather–climate (Zhang 2013). Its global importance has motivated many studies during nearly a half century (Jiang et al. 2020; Zhang 2005). However, few global climate models can adequately reproduce the MJO (Ahn et al. 2017, 2020; Jiang et al. 2015) and the fundamental MJO dynamics is still debatable (Zhang et al. 2020). In contrast to the equatorially trapped waves that are well represented by a set of analytical solutions to linear shallow-water equations on an equatorial β plane (Matsuno 1966), there has not been an MJO solution to these equations. This has motivated many to seek an alternative set of equations that may yield an MJO solution to explain its fundamental dynamics, namely, mechanisms for the selection of its intraseasonal and planetary scales and eastward propagation. Such a quest to theoretically understand the MJO has been considered a ''holy grail'' of research on the tropical atmosphere (Raymond 2001).

The first attempt at theoretically explaining the MJO (Chang 1977) focused on whether and how the eastward-propagation speed of the equatorial Kelvin wave, one of Matsuno's solutions, might be slowed down by viscosity to that of the observed MJO. This attempt demonstrated that when viscous damping is added to the Matsuno's equations, the speed of the equatorial Kelvin wave is indeed slowed down but the corresponding solution does not match the observed MJO. Since that study, there have been several others that intended to explain the MJO in terms of various dynamic mechanisms. These mechanisms include gravity waves (Yang and Ingersoll 2013, 2014), nonlinear solitary waves (Rostami and Zeitlin 2019; Yano and Tribbia 2017), and large-scale vortex (Hayashi and Itoh 2017). These mechanisms may include atmospheric convection implicitly or explicitly as energy sources, but their dynamics is essentially dry, meaning they do not use any moisture equation or even any moisture variable.

Parallel to these dry-dynamical approaches, many have adapted a notion that the fundamental dynamics of the MJO is anchored on moisture. The reasons for this notion come from several angles. In observations, signals of the MJO in atmospheric convection and precipitation are not separable from those in its circulations, at least over the Indo-Pacific warm pool where the strongest MJO signals are. Signals of the MJO in moisture have been repeatedly observed (Kemball-Cook and Weare 2001; Kikuchi and Takayabu 2004; Kiladis et al. 2005; Lin and Johnson 1996; Myers and Waliser 2003; Weare 2003).

Corresponding author: Ji-Eun Kim, jieunkim@pusan.ac.kr

DOI: 10.1175/JAS-D-20-0193.1

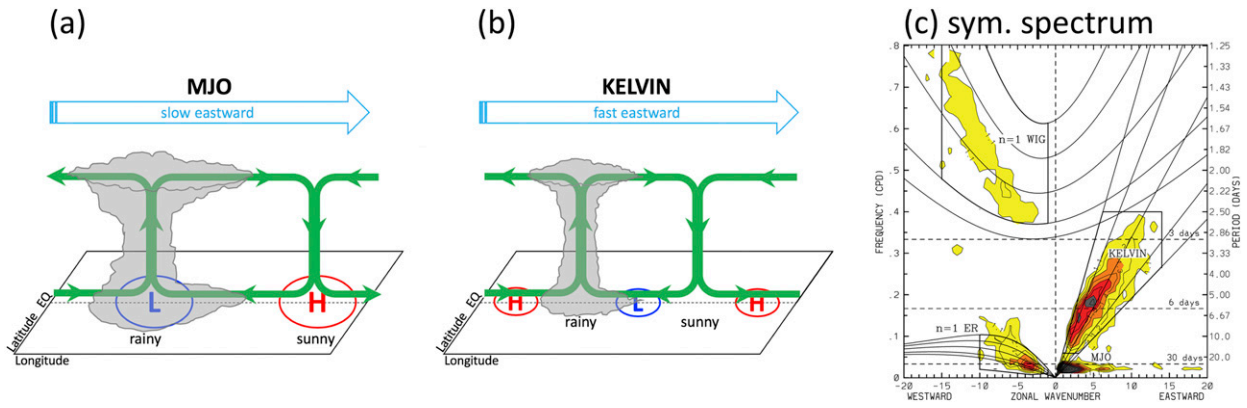

FIG. 1. Schematic of wind–pressure phase relations for (a) the MJO and (b) Kelvin waves. (c) Observed wavenumber–frequency spectrum of the equatorial symmetric component of brightness temperature [(c) is reproduced from Kiladis et al. (2009)].

The close connection between moisture and convection or precipitation (Bretherton et al. 2004) has led to a realization that moisture must be considered as part of the convection–circulation coupling of the MJO. Moisture has been incorporated in MJO theories, from the early boundary layer frictional convergence theory (Wang 1988b; Wang and Rui 1990) to the recent all-included trio-interaction theory (Wang et al. 2016) and scale-interaction theories (Biello and Majda 2005; Majda and Stechmann 2009b). Another motivation to include moisture in MJO theories is the fact that the spectral signals of the MJO and Kelvin waves appear to be different, and that there is no MJO in the Matsuno's solutions to dry shallow-water equations. If the MJO were another mode of variability in addition to Matsuno's solutions to shallow-water equations, then an additional variable would be needed to derive an MJO solution. Moisture has been commonly selected as this additional variable. Under the concept of gross moisture stability (Neelin et al. 1987; Raymond and Fuchs 2009), the role of moisture in the MJO has reached its pinnacle in a moisture mode theory, in which the only prognostic equation needed to produce an MJO solution is that of moisture (Adames and Kim 2016). These variety of thinking and approaches in theoretical understanding of MJO dynamics highlight the healthy growth in the MJO study and meanwhile indicate the issue is far from being settled.

In this current study, we intend to add another piece to the existing rich pool of ideas on MJO dynamics. Our objective is to use possibly the simplest mathematical framework to find an analytical solution that may explain the most fundamental features of the MJO, namely, its planetary and intraseasonal scales and eastward propagation. We consider the mechanism for these features the core dynamics of the MJO. We revisit Chang's (1977) idea of including momentum damping to seek an analytical solution that may interpret the MJO as slowed-down Kelvin waves. We use the linear equatorial shallow-water equations that have a constant equivalent depth similar to the approach of Matsuno (1966) except linear damping of zonal wind is included.

Because the MJO and Kelvin wave are commonly viewed as two distinct phenomena, using the latter to explain the former requires justifications, which are given in section 2. After a brief introduction of the method and data used in this study in section 3, we present in section 4 an analytical solution to the Matsuno's equatorial shallow-water equations with momentum damping and demonstrate how this solution predicts the most fundamental features of the MJO and additional observed structure of the MJO. We illustrate how this solution can represent both the MJO and Kelvin waves depending on the scale of the perturbations. We also use the same mathematical framework to explore the role of external forcing and feedback for the MJO in section 5. Further discussions are given in section 6 on the choice of damping scales, the role of Rossby waves in the MJO, which are omitted in our MJO solution, and comparisons between our and other MJO theories. Concluding remarks are given in section 7.

2. MJO and Kelvin waves

The observed differences between the MJO and Kelvin waves[1] in their zonal scales, periods, and hence propagation speeds are well known. There are also other observed differences between the MJO and Kelvin waves. Zonal wind and geopotential (or pressure) in the lower troposphere are in phase for the Kelvin waves (Fig. 1b) but they are in quadrature for the MJO (Fig. 1a).[2] In terms of the horizontal structure, the MJO expands away from the equator in a swallowtail pattern, while Kelvin waves are more confined to the equator with a much subtler swallowtail pattern than the MJO (Adames and Wallace 2015; Zhang and Ling 2012). Their spectral power peaks appear to be separated (Wheeler and Kiladis 1999).

[1] The theoretical dry Kelvin waves and observed convectively coupled or moist Kelvin waves are not distinguished in this study because, except for phase speeds, their differences are much smaller than the differences between them and the MJO.

[2] It should be pointed out that the first baroclinic structures in Figs. 1a and 1b are too simplistic. The wind–pressure phase relationship of the MJO in the upper troposphere is closer to that of the Kelvin waves than in the lower troposphere (e.g., Roundy 2019).

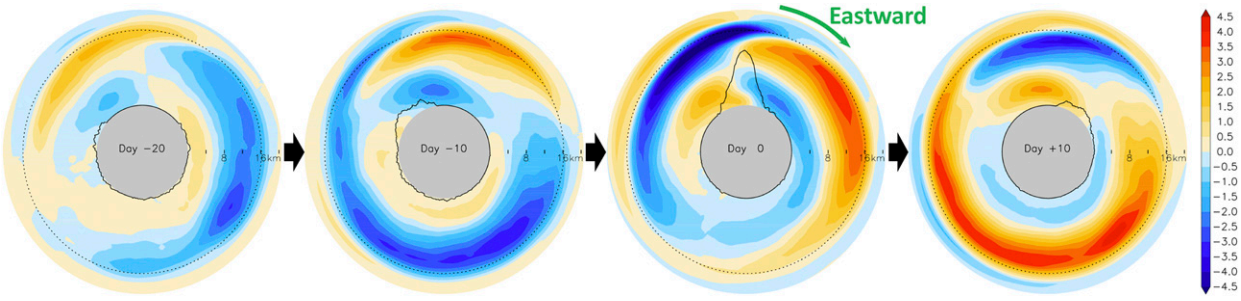

FIG. 2. Circular longitude–height representation of the MJO. Gray central circles represent the equatorial cross section of Earth. Blue and red colors are, respectively, atmospheric easterly and westerly winds ($m\,s^{-1}$) from the surface to 22 km. The atmospheric depth is disproportional relative to Earth's radius for the purpose of visualization. Dotted lines indicate the approximate location of the tropopause (100 hPa). Zonal winds are composited against TRMM precipitation (black contours around the gray circles) between 10°S and 10°N and for each 10° longitude bin, with its peaks representing MJO convection centers (see section 3). Then seven 10° longitude bins between 80° and 150°E are averaged. Arrows mark the time sequence. A spiral shape of the easterly and westerly wind pair moves eastward (clockwise) with enhanced rainfall (day 0), but the wind signal circumnavigates even for periods of no significant convection (e.g., days −20 to −10). The wind pair indicates that the MJO is a zonal wavenumber 1 phenomenon even its convection is localized. Patterns for days −20 and +20 (not shown) are very similar.

The global appearance of signals in MJO wind is its unique feature that does not exist in other zonally propagating perturbations in Earth's atmosphere. These planetary scale (zonal wavenumber $k = 1$) structures of the MJO in both lower and upper troposphere are connected not only in the region of MJO convection but also in regions far away from an MJO convection center (Fig. 2). In contrast, Kelvin waves are regional phenomena at a given time (Kiladis et al. 2009). Given these distinctions between the MJO and Kelvin waves, why would anyone even try to use the Kelvin wave to explain the MJO? This question can be answered from the perspective of one of the most fundamental issues of the MJO: Why does it propagate eastward?

In the literature, the eastward propagation of the MJO is often explained in terms of higher moisture in the boundary layer and lower troposphere east of an MJO convection center than west of it. This moisture distribution relative to an MJO convection center has been commonly observed (Benedict and Randall 2007; Johnson et al. 2015; Kemball-Cook and Weare 2001; Kiladis et al. 2005), reproduced by a few global climate models (Jiang et al. 2015), and predicted by a number of MJO theories (Adames and Kim 2016; Majda and Stechmann 2009b; Wang and Rui 1990; Wang et al. 2016). This explanation of eastward propagation of the MJO in terms of the low-level moisture distribution appears to be convincing because development of new convection east of an existing MJO convection center would be more favored than west of it, leading to eastward propagation of the convection center and the entire MJO. This explanation is, however, not very satisfactory. An apparent counterargument would be, Why does not this zonal distribution of low-level moisture occur in reverse so the MJO would propagate westward? A deeper explanation is needed.

The only reason for the zonal asymmetry in low-level moisture of the MJO, namely, the moisture increase east of an MJO convection center and decrease west of it, is the asymmetry of the Kelvin wave structure to the east and the Rossby wave structure to the west of an MJO convection center. With few exceptions, MJO theories that predict the zonal asymmetry in moisture as the mechanism for the eastward propagation of the MJO include both the Kelvin and Rossby wave components (Adames and Kim 2016; Lau and Peng 1987; Majda and Stechmann 2009b; Wang and Rui 1990; Wang et al. 2016). In this study, we will show that without the Rossby wave component, the MJO can still propagate eastward at its observed speed when momentum damping is included to slow down the Kelvin waves.

Kelvin waves are a special type of gravity wave propagating along a boundary, prohibiting fluid motion perpendicular to the boundary. Similar to the unidirectional coastal Kelvin waves along a topographic boundary, equatorial Kelvin waves exist because of changing sign of the Coriolis force at the equator that serves as a boundary of fluid motion, thus prohibiting meridional velocity. Kelvin waves are nondispersive, implying that the phase speed must remain constant at all scales. A recent study using topology (Delplace et al. 2017) further provides a mathematical basis for the existence of Kelvin waves at $k = 1$. The study shows that the equatorial Kelvin waves are topological edge states due to time-reversal symmetry breaking by Earth's rotation. Edge states are topologically protected modes, meaning that the existence of the modes is robust against any perturbations to a system such as topological defects and impurities (Moore 2010). In Earth's atmosphere, because the equatorial Kelvin modes are topologically protected, Kelvin waves must be excited especially at low zonal wavenumbers regardless of complicated interactions among various elements (e.g., circulations, convective heating, moisture, radiation, surface fluxes, boundary layer dynamics, eddies). Therefore, the lack of observed Kelvin waves at $k = 1$ and the strong observed signal of the MJO at $k = 1$ in the tropical circulation (Fig. 2) suggest that the MJO is fundamentally a modified $k = 1$ Kelvin wave.

The distinct features of the Kelvin waves and MJO discussed above nonetheless, there are observations showing

their continuum nature (Roundy 2012). The circumnavigating propagation of the MJO shown in Fig. 2 and previously by others (Gottschalck et al. 2013; Kiladis et al. 2005; Powell 2017; Virts and Wallace 2014), especially in the case of successive MJO events (Matthews 2008), has been viewed as a transition from the MJO to the Kelvin wave over the eastern Pacific and then from the Kelvin wave to the MJO over the Indian Ocean (Powell 2017; Sakaeda and Roundy 2016; Sobel and Maloney 2012). When individual eastward-propagating large-scale convective events are identified, their propagating speeds range continuously from 0 to greater than 10 m s^{-1} without any distinct separation between those of the MJO and those of Kelvin waves (Zhang and Ling 2017). The seemingly distinct enhanced spectral signals between the MJO and Kelvin waves (Fig. 1c) are largely attributed to geographical variations of convection and extratropical influences (Roundy 2012, 2014). This spectral separation in the global signal may not exist regionally (Roundy 2012). Moreover, the typically practiced spectral method (Wheeler and Kiladis 1999) to remove red background noise eliminates more of the continuous spectral signal between the MJO and Kelvin waves (Roundy 2019).

In short, the MJO and Kelvin waves are two distinct phenomena but the transition between them is smooth and continuous. A theory that explains the MJO based on Kevin waves must be able to demonstrate both their distinctions and continuum nature. This is what we intend to do in the next sections.

3. Data and methods

We use linear shallow-water equations on an equatorial β plane, similar to those used by Matsuno (1966), and seek their analytical solutions to represent the MJO. The solutions of different wavenumbers will be compared with the observed MJO and equatorial Kelvin waves to assess the extent to which these perturbations can be represented by the solutions. The analytical solutions are validated against daily rainfall from the Tropical Rainfall Measuring Mission (TRMM) 3B42 v7 (Huffman et al. 2007), and geopotential and winds at 850 hPa from the European Centre for Medium-Range Weather Forecasts interim reanalysis (ERA-Interim) (Dee et al. 2011). Both data are interpolated to horizontal grids of 1° × 1°, and cover February 1998–January 2015. The outgoing longwave radiation (OLR) MJO index (OMI) of Kiladis et al. (2014) is also used. MJO events are identified by the following procedure: 1) the TRMM rainfall data are averaged over latitudes of 10°S–10°N and each 10° longitude bin; 2) the time series of precipitation from 1 is smoothed by applying 10-day running mean; 3) a peak in smoothed rainfall from 2 is identified by detecting a change in the sign of its tendency; and 4) a peak from 3 is selected as associated with the MJO if its value and the corresponding OMI are both greater than their perspective one standard deviation. Variables for selected MJO events are averaged into their composites. The use of the TRMM data and OMI in combination captures the planetary scale and eastward-propagating signals of the MJO as well as its local signals in precipitation. A similar method is used for Kelvin waves, except a Kelvin wave filter, shown in Fig. 1c, is first applied to the data instead of the smoothing.

4. MJO as a harmonic oscillator

We start with slightly modified Matsuno's equations for Kelvin waves (zero meridional velocity) by adding Rayleigh momentum damping to the equation of the zonal velocity:

$$\frac{\partial u}{\partial t} + Du + \frac{\partial \phi}{\partial x} = 0, \tag{1}$$

$$\beta y u + \frac{\partial \phi}{\partial y} = 0, \tag{2}$$

$$\frac{\partial \phi}{\partial t} + gH\frac{\partial u}{\partial x} = M, \tag{3}$$

where u is zonal velocity, ϕ geopotential, H the equivalent depth, D a linear damping coefficient, β the latitudinal derivative of the Coriolis parameter, g the gravitational acceleration, M the mass source/sink treated as external forcing, x longitude, y latitude, and t time. Without damping and the mass source, Eqs. (1)–(3) yield the classical Kelvin wave solution of Matsuno (1966). With damping, they give a solution that still propagates eastward but with different characteristics from the Kelvin waves on the planetary scale (zonal wavenumber $k = 1$). In the following, we demonstrate how damping reduces the frequency of the classical Kelvin waves to intraseasonal values and transforms the horizontal structure of the Kelvin waves to one that is similar to the observed MJO but only at the planetary scale. We interpret this planetary scale, intraseasonal, and eastward-propagating perturbation under the influence of damping as the core dynamics of the MJO.

a. Role of damping in frequency reduction

Combining Eqs. (1) and (3) leads to

$$\frac{\partial^2 u}{\partial t^2} + D\frac{\partial u}{\partial t} - gH\frac{\partial^2 u}{\partial x^2} = -\frac{\partial M}{\partial x}. \tag{4}$$

Assuming a wave solution in the zonal direction $u(t)e^{ikx}$, and replacing $-\partial M/\partial x$ with X for simplicity, Eq. (4) becomes

$$\frac{\partial^2 u}{\partial t^2} + D\frac{\partial u}{\partial t} + \omega_0^2 u = X, \tag{5}$$

where $\omega_0 = k\sqrt{gH}$ is the natural frequency of the classical Kelvin waves when both D and X are zero. Equation (5) is exactly the same as the universal equation for damped harmonic oscillators such as spring motions, pendulums, and electric circuits under effects of friction or resistance. The damped harmonic oscillator has two standard solutions. One is a transient solution when $X = 0$:

$$u_{\text{transient}}(x,t) = u_0 e^{-(D/2)t} e^{i(kx-\omega_D t)}, \tag{6}$$

where

$$\omega_D = \sqrt{\omega_o^2 - D^2/4} = \sqrt{gHk^2 - D^2/4} \tag{7}$$

is the reduced frequency from ω_0 by damping D. The time evolution of this solution critically depends on the damping ratio, $D/(2\omega_0)$. The amplitude exponentially decays without oscillation if $D/(2\omega_0) > 1$ (overdamped), but otherwise gradually decays with an oscillation at frequency ω_D.

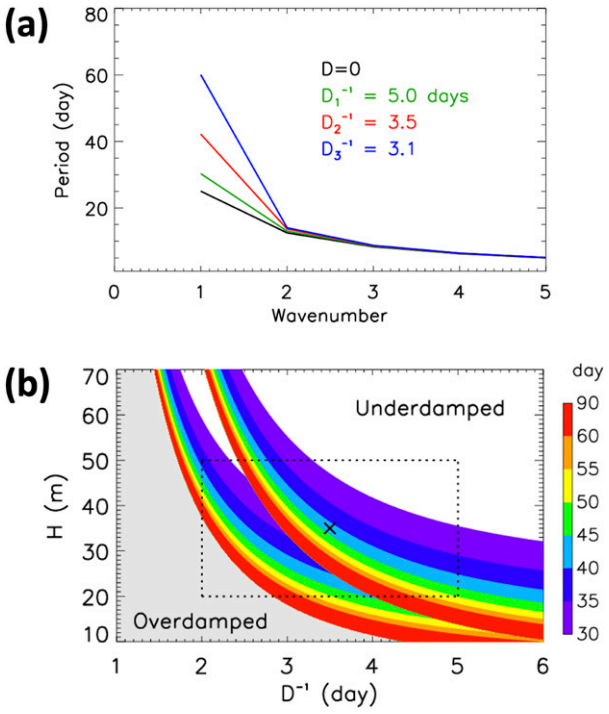

FIG. 3. (a) Theoretical period as a function of zonal wavenumber, calculated for the steady-state resonant solution with $H = 35$ m for different damping scales. (b) Theoretical periods (colors) of $k = 1$ solutions as functions of damping time scale D^{-1} and equivalent depth H. The left rainbow is for the transient solution and the right one is for the steady-state resonant solution. No oscillation exists in the gray area (overdamped). Periods are shorter than 30 days in the white area (underdamped). The area enclosed by the dotted rectangle corresponds to commonly observed ranges of damping coefficients and equivalent depths. The cross in the center of the rectangle marks the values of the equivalent depth ($H = 35$ m) and damping ($D^{-1} = 3.5$ days) used throughout this study.

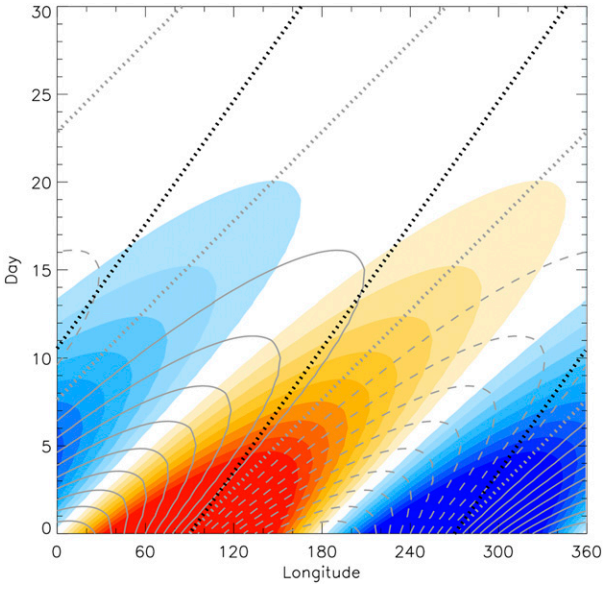

FIG. 4. Longitude–time diagram of convergence (red), divergence (blue), and zonal wind u (contours; gray dotted for zero, solid for positive, and dashed for negative, with intervals of 0.1 m s^{-1}) from the transient solution of a damped harmonic oscillator for $k = 1$, $H = 35$ m, and $D^{-1} = 3.5$ days. An initial perturbation amplitude of $u_0 = 1$ m s^{-1} is imposed. Black dotted lines represent zero wind for a resonant solution.

When nonzero X oscillates at frequency ω, the system can oscillate with a steady-state amplitude. The solution is

$$u(x,t) = u_0 e^{i(kx-\omega t)}, \tag{8}$$

where

$$u_0 = \frac{X_0}{\sqrt{(\omega^2 - \omega_0^2)^2 + D^2\omega^2}}. \tag{9}$$

This amplitude reaches its maximum when the frequency of X matches the system's resonance frequency:

$$\omega_R = \sqrt{\omega_o^2 - D^2/2} = \sqrt{gHk^2 - D^2/2}. \tag{10}$$

Similar to ω_D of the transient solution, an important effect of damping is to reduce the natural frequency ω_0 to the resonant frequency ω_R that allows a maximum response to external forcing. This resonant frequency is an intrinsic property of the oscillator and is independent of the external forcing (not a function of external forcing's frequency or strength). The effect of damping on the reduced frequencies ω_D and ω_R depends on the equivalent depth H and zonal wavenumber k. For example, with $H = 35$ m, which is within its observed range of 12–50 m for the tropical atmosphere (Kiladis et al. 2009), the resonant period $2\pi/\omega_R$ increases with decreasing k and also increases with damping but only at $k = 1$ (Fig. 3a). The period of the transient solution $2\pi/\omega_D$, is slightly shorter than that of the resonant solution and behaves similarly with k. At $k = 1$ and with damping time scales $D^{-1} = 3$–5 days, the solutions oscillate at periods of roughly 30–60 days. These are the periods of the observed MJO. At $k = 1$, there is a range of H and D that would result in frequencies (periods) similar to those of the observed MJO (Fig. 3b). At a given damping scale, a response period becomes longer for smaller H, which is equivalent to lower effective static stability of the atmosphere. At a given H, a response period becomes longer with stronger damping. There is no resonant oscillation if damping is too strong ($D^2 > 2gHk^2$).

Damping is effective only at the planetary scale ($k = 1$) when $D^{-1} = 3$–5 days for an average value of observed H, and becomes negligible at higher wavenumbers because the higher wavenumbers corresponds to higher natural frequencies ω_o. If damping is too strong ($D^{-1} \ll \sim 3$ days) compared to the natural frequency, perturbations of $k = 1$ either do not oscillate (the gray area in Fig. 3b) or decay too quickly resulting in nearly no oscillation. This selection mechanism for the zonal scale, shown in Fig. 3a, provides a sweet spot in the dispersion relationship of the resonant solution in Eq. (10) for intraseasonal frequencies.

In Fig. 4, we demonstrate how $k = 1$ transient and resonant solutions evolve with the damping time scale of 3.5 days.

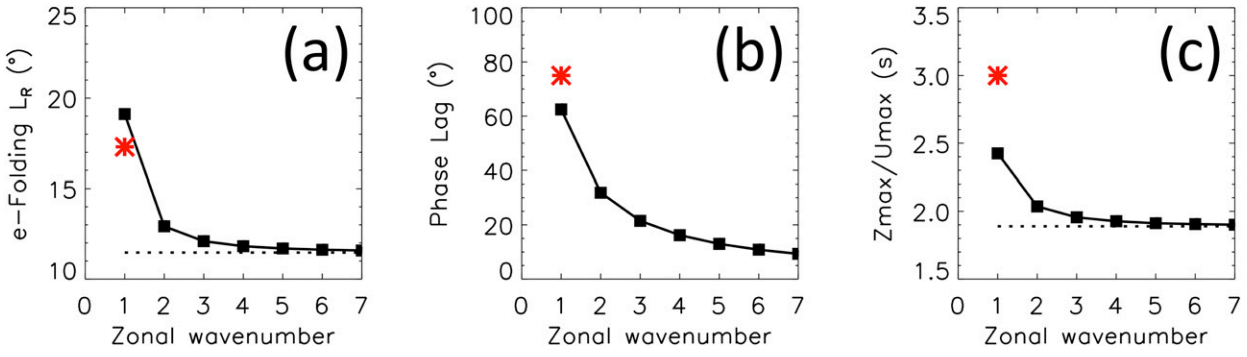

FIG. 5. Theoretical results of (a) e-folding decay width L_R as a function of wavenumber for $H = 35$ m and $D^{-1} = 3.5$ days, (b) phase difference between geopotential height and zonal wind, and (c) the ratio of the maximum amplitude of geopotential height to that of zonal wind. Dotted lines are for $D = 0$. Asterisks correspond to observed values of the MJO, calculated from the composite analysis (section 3).

Even though its amplitude decays with time, the transient solution can still exhibit the eastward wave feature. The two dotted lines in Fig. 4 compare propagation speed and period for the transient (gray) and resonant (black) solutions. Different slopes of these lines suggest that without external forcing the transient solution would be a weaker single event and propagates faster than the resonant solution. Thus, the transient [Eq. (6)] versus resonant [Eq. (8)] solution predicts that strong perturbation events would propagate slower, have longer periods, and tend to have multiple successive events. This turned out to be true in observations of the MJOs between the easterly and westerly stratospheric quasi-biennial oscillation (QBO) (Son et al. 2017), although how the stratosphere interacts with convection is another subject of research.

The choice of using $D^{-1} = 3.5$ days to demonstrate the behaviors of our solutions is justified in section 6a.

b. Phase and amplitude relationships between ϕ and u

Plugging a general wave solution $e^{i(kx-\omega t)}$ into Eq. (1) results in a phase lag and amplitude ratio between ϕ and u:

$$\mathrm{Re}(u) = u_0 \cos\theta, \tag{11}$$

$$\mathrm{Re}(\phi) = u_0 A \cos(\theta + \theta_{\mathrm{lag}}), \tag{12}$$

where u_0 is the amplitude of u, θ a phase of u, $A = \sqrt{\omega^2 + D^2}/k$ an amplitude ratio of ϕ to u, and $\theta_{\mathrm{lag}} = \tan^{-1}(D/\omega)$ a phase difference between ϕ and u. With a given D, ϕ lags u. For $\omega = \omega_R$, this phase lag increases as k decreases (D/ω_R increases). With $D^{-1} = 3.5$ days, θ_{lag} is about a quarter of cycle at $k = 1$ (Fig. 5b). This quadrature phase relationship between ϕ and u is observed for the MJO (Fig. 6a). It makes a low pressure center collocated with convergence resulted from the lower-tropospheric easterly–westerly transition. This provides a dynamic structure for a strong role of moisture convergence in the MJO as suggested by some of the MJO theories. At higher k ($D/\omega_R < 1$), the lag almost disappears, which is observed for the Kelvin waves (Fig. 6b). In this case, there is no collocation between a low pressure center and convergence, which would make moisture feedback less important to the Kelvin waves.

c. Meridional structure and eastward propagation

To solve for the meridional structure of the harmonic oscillator, we combine Eqs. (1) and (2) into

$$\frac{\partial^2 u}{\partial y \partial t} + D\frac{\partial u}{\partial y} - \beta y \frac{\partial u}{\partial x} = 0 \tag{13}$$

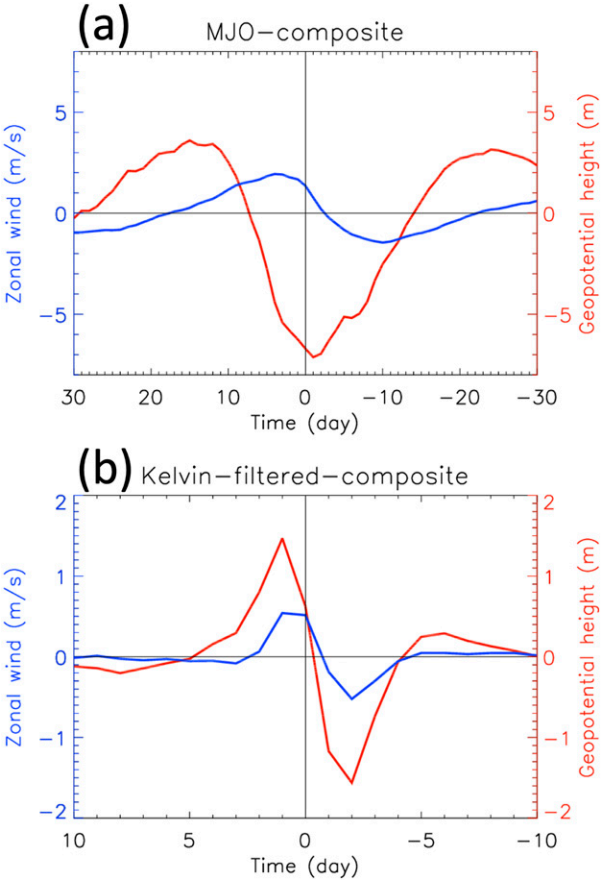

FIG. 6. Composites of observed zonal wind (blue) and geopotential height (red) at 850 hPa with respect to time for (a) the MJO and (b) Kelvin waves (see section 3 for details).

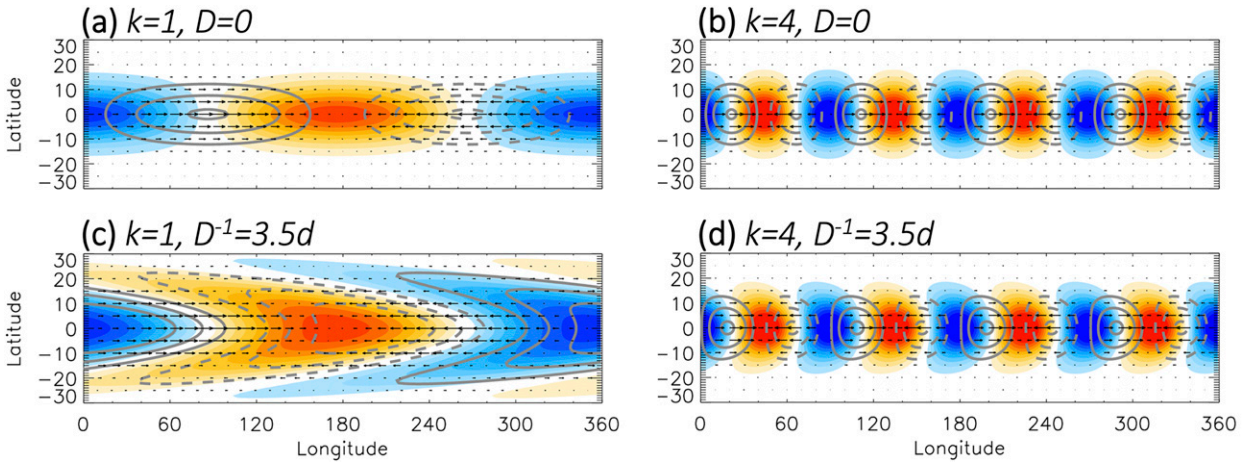

FIG. 7. Snapshot of the full resonant solution $u(y)e^{i(kx-\omega_R t)}$ for (a) $k = 1$ and $D = 0$, (b) $k = 4$ and $D = 0$, (c) $k = 1$ and $D^{-1} = 3.5$ days, and (d) $k = 4$ and $D^{-1} = 3.5$ days. Color represents convergence (red) and divergence (blue) with arrows being zonal winds. Gray solid (positive) and dashed (negative) contours are geopotential.

and insert $u(x, y, t) = u(y)e^{i(kx-\omega t)}$ into Eq. (13). This yields

$$u(y) = e^{-l^2y^2}e^{im^2y^2}, \tag{14}$$

where $l^2 = \beta c_r/2(c_r^2 + c_i^2)$ and $m^2 = \beta c_i/2(c_r^2 + c_i^2)$ with $c_r = \omega/k$, $c_i = D/k$. Here l and m stand, respectively, for a meridional decay scale and meridional wavenumber. When $D = 0$, Eq. (14) reduces to $u(y) = e^{-\beta y^2/2c_0}$ where $c_0 = \omega_0/k$, which is for the classical Kelvin waves with its horizontal structure (Figs. 7a,b) identical to that obtained by Matsuno (1966).

In the presence of damping ($D \neq 0$), similar to the classical Kelvin waves, only a positive zonal phase speed $c_r = \omega/k$ leads to a physically possible state in the meridional direction (exponentially decaying away from the equator), and westward propagation ($c_r < 0$) must be ruled out because its amplitude increases exponentially with latitude.

The combination of the real and imaginary parts of the meridional solution in Eq. (14) indicates that, with damping ($D \neq 0$), the perturbation propagates away from the equator with an exponentially decreasing amplitude. This theoretical prediction is shown in the latitude–time diagram for zonal wind and convergence/divergence compared to observed wind and precipitation in Fig. 8. The combination of all imaginary parts $[e^{i(kx+m^2y^2-\omega t)}]$ of the full solution expresses northeastward phase propagation in the Northern Hemisphere and southeastward in the Southern Hemisphere (Fig. 8a). Studies have indeed observed the northeastward propagation of the intraseasonal oscillation during boreal summer (Jiang et al. 2004; Sikka and Gadgil 1980; Yasunari 1979, 1980), and the southeastward propagation during boreal winter (Jiang et al. 2004). Although a warmer tropical hemisphere in a given season shows more prominent poleward propagation with stronger intraseasonal activity, a colder hemisphere also exhibits poleward propagation in observations (Jiang et al. 2004; Kemball-Cook and Wang 2001; Meehl et al. 2020; Qi et al. 2019) (Figs. 8b,c). Easterly (dashed line) followed by convergence

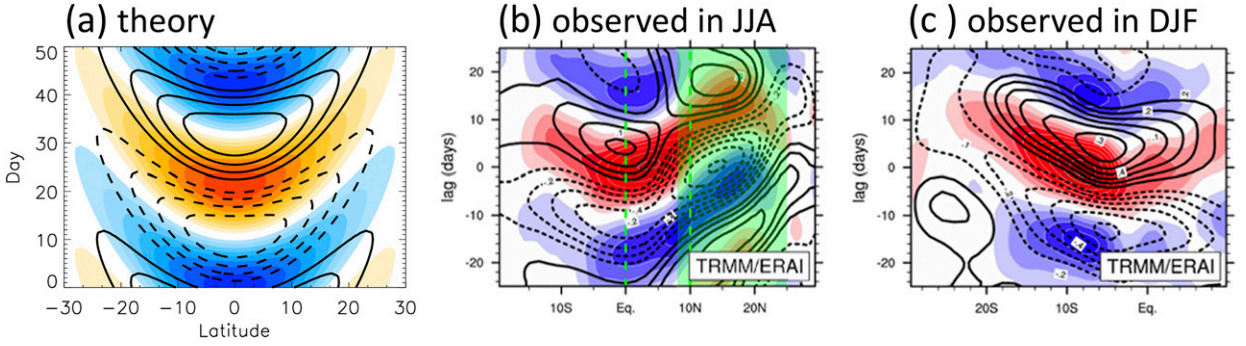

FIG. 8. Latitude–time diagrams of (a) the full resonant solution for $k = 1$, $H = 35$ m, and $D^{-1} = 3.5$ days, and observed composites of the MJO in (b) boreal summer and (c) boreal winter. Color represents convergence (red) and divergence (blue) in (a), and positive (red) and negative (blue) precipitation anomalies of TRMM observations in (b) and (c). Contours corresponds to westerly (solid) and easterly (dashed) anomalous wind from the theory in (a) and from ERA-Interim in (b) and (c). The values in (b) are calculated as lag correlation of TRMM precipitation averaged over 0°–10°N, 80°–100°E, and similarly (c) is lag correlation against precipitation over 15°S–0°, 60°–90°E [(b) and (c) are reproduced from Meehl et al. (2020)].

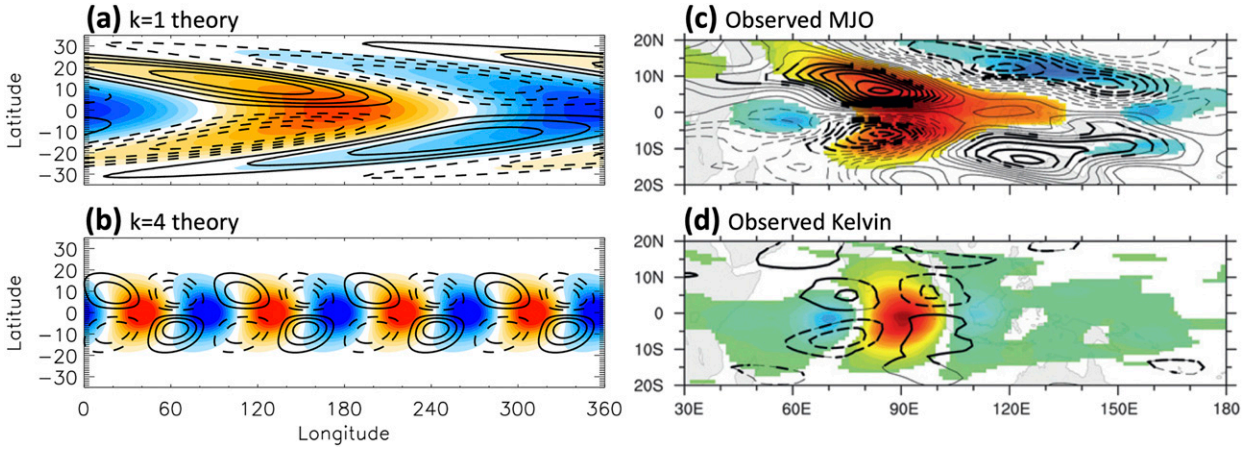

FIG. 9. (a) Theoretical horizontal distribution of convergence (red), divergence (blue), and vorticity anomalies (contours; solid for positive and dashed for negative) for the resonant solution with $k = 1$, $H = 35$ m, and $D^{-1} = 3.5$ days. (b) As in (a), but for $k = 4$. (c) Observed horizontal structure of precipitation anomalies (red for positive and blue for negative) and potential vorticity (contours) of the MJO. (d) As in (c), but for Kelvin waves [(c) and (d) are from Zhang and Ling (2012)].

(red in Fig. 8a) or enhance precipitation (red in Figs. 8b,c) is consistently shown in both theory and observations. This provides another piece of evidence that adding the damping effect to the linear shallow-water equations under stochastic forcing is sufficient to reproduce fairly similar wave characteristics to observations. In other words, similar to the essential role of damping on the emergence of the new time scale (section 4a) and different responses of fields (section 4b), the emergence of poleward propagation is also attributed to damping.

The poleward phase propagation can be further depicted in a snapshot of the horizonal structure of $k = 1$ and $\omega = \omega_R$ in Figs. 7c and 9a. The meridionally slanted structure forms a swallowtail pattern in geopotential and wind divergence $\partial u/\partial x$ (Fig. 7c), and vorticity $\partial u/\partial y$ (Fig. 9a). The swallowtail pattern has been observed in many fields associated with the MJO such as precipitation and potential vorticity (Fig. 9c), moisture, winds, geopotential, temperature, vorticity, and boundary layer convergence (Adames and Wallace 2014, 2015; Zhang and Ling 2012). The observed potential vorticity in Fig. 9c and the theoretical vorticity in Fig. 9a share similarities in both their shapes and relative phases to convection (red), represented by precipitation in the observation and by convergence in the theory. The MJO's swallowtail pattern has been explained in terms of boundary layer convergence (Wang et al. 2016) or the equatorial Rossby waves (Adames and Kim 2016). Here, we demonstrate that this pattern can exist with neither boundary layer convergence nor the Rossby waves. The Rossby waves associated with the MJO will be further discussed in section 6b.

The swallowtail pattern becomes less evident as k increases. At $k = 4$, for example, it still exists, however subtle it might be (Figs. 7d and 9b), but completely disappears without damping (Fig. 7b). This subtle swallowtail pattern has been observed for the tropospheric Kelvin waves (Fig. 9d) (Zhang and Ling 2012). The similar structures between the theoretical solutions with damping and observations for the MJO and Kelvin waves (Fig. 9) constitute a strong testament of the damping effect present in the atmosphere and serve as a validation of our approach to understand the most fundamental dynamics of the MJO.

Results presented in this section demonstrate that the simple solutions of damped harmonic oscillators capture the most fundamental features of the MJO, namely, its planetary and intraseasonal scales and eastward propagation. Our solutions also capture certain observed horizontal structures of the MJO including poleward propagation with a swallowtail pattern. Because our solution captures the most fundamental features of the MJO but not its every aspect in observations, we take the solution as the core dynamics of the MJO. Our solution indicates that the existence of the MJO is rooted in dynamics in the presence of zonal momentum damping but without explicit moisture variability.

The MJO can exist with or without external forcing, but sustained MJO events require external forcing or energy sources. In the next section, we extend our analysis to see to what degree the simple mathematical framework we are using may reveal the role of external forcing and feedback processes as energy sources of the MJO.

5. Energy sources

When the damping time scale is too short compared to the MJO time scales, a given large-scale perturbation decays quickly if no additional force is applied. As shown in Fig. 4, the decaying transient solution only exhibits a single large-scale convection event (represented by convergence) due to damping. While there are observed cases of such decaying MJO events, typically observed MJO events last longer than the damping time scale, indicating both the transient and steady-state solutions can exist. The term X in Eq. (5) for typical MJO events can be estimated from budget calculations of the left-hand side of Eq. (5) (see discussion below). Its nonzero values indicate the presence of energy sources for typical MJO events. In section 4, we discussed the intrinsic properties of the MJO solution in the presence of external forcing but without any specific information

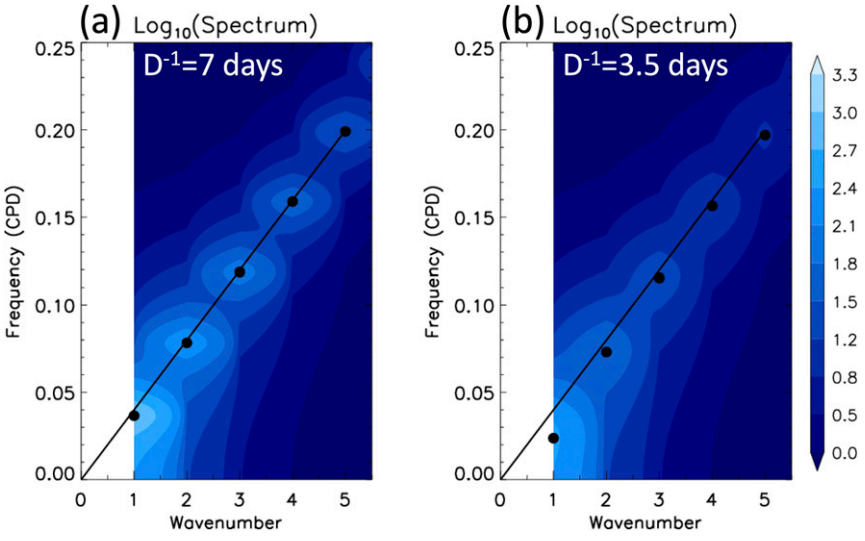

FIG. 10. Theoretical power spectrum of resonant solutions in response to Gaussian white noise forcing for $H = 35$ m and (a) $D^{-1} = 7$ days and (b) $D^{-1} = 3.5$ days. Black dots correspond to spectral maxima at ω_R for individual wavenumbers. The black line is the Kelvin dispersion curve for $D = 0$.

of the forcing. In this section we further discuss the MJO solution with characteristics of external forcing in consideration (section 5a). We also discuss possible roles of feedback processes in the core dynamics of the MJO (section 5b).

a. External forcing

Because the resonant frequency ω_R is independent of external forcing, any forcing with energy power at ω_R would lead to resonant response of the MJO. Stochastic processes, such as white or red noise, would suffice to excite the MJO. Stochastic forcing may come from perturbations in air–sea fluxes and convective activity in the tropics. For example, strong but random deep convection in the tropics generates a broad scale of wave excitations, which then resonate and be amplified at intrinsic wave frequencies. Mass fluxes from multiscale moist convection (Moncrieff 1992) may contribute to mass sources, thus works as a driving force of the oscillation system. Also, independent perturbations from the extratropics may penetrate into the tropics and serve as energy sources to the MJO (Frederiksen and Lin 2013; Hsu et al. 1990; Lau et al. 1994; Matthews et al. 1996; Ray et al. 2009).

Responses to stochastic forcing takes a form similar to the response to forcing of a single frequency as shown in Eq. (9) (Hashemi 2016; Masoliver and Porrà 1993). We demonstrate the damping effect on periods of the harmonic oscillator in the presence of Gaussian white noise forcing in Fig. 10. The spectral power at resonance (at black points in Fig. 10) increases as k decreases for given D, and the changes in power at different wavenumbers increase with stronger damping [due to $D^2\omega^2$ in Eq. (9)], demonstrating the zonal-scale selection by damping. The resonant frequency shifts from short periods with weak damping of $D^{-1} = 7$ days (Fig. 10a) to longer ones with stronger damping of $D^{-1} = 3.5$ days (Fig. 10b), indicating that damping acts to provide a mechanism for the temporal-scale selection of the harmonic oscillator. The similarity between the spectral response in Fig. 10b and observed spectra of tropical variables such as zonal wind and precipitation demonstrates that white noise forcing is sufficient to induce the enhanced spectrum at the MJO scale. Interestingly, the theoretical spectrum in Fig. 10b further suggests that larger and lower-frequency tropical waves would have stronger signals in spite of white forcing due to stronger amplification at these scales. This might explain why the tropical wave spectrum itself has red properties (Roundy 2019). Our solution that includes both the MJO and Kelvin waves, and their expected spectrum in Fig. 10b support the notion of the MJO–Kelvin wave continuum (Roundy 2012, 2019). For given external forcing X, the peak of the spectral power of the MJO would be further enhanced if X is stronger [larger X_0 in Eq. (9)] at scales that are close to those of the MJO.

In addition to the amplitude response u_0 to external forcing in Eq. (9), additional information on the phase of the responses is also well-known. When a system has nonzero damping, there is a time lag between the wave response and its external forcing:

$$\theta_{u-X} = \tan^{-1}\left(\frac{D\omega}{\omega^2 - \omega_0^2}\right), \tag{15}$$

where θ_{u-X} is the phase lag between u and X. Equation (15) describes that the response is in phase with external forcing when damping is absent. X can be estimated as the residual of Eq. (5) using observations. The composites of u and X shown in Fig. 11 reveal that u lags about 5–6 days behind X. When values of $D^{-1} = 3.5$ days and $H = 35$ m are used in Eq. (15), θ_{u-X} becomes 5.4 days, which is consistent with what is observed in Fig. 11. The theoretical amplitude ratio $u_0/X_0 \sim 17\,\text{day}^{-2}$ calculated using Eq. (9) is also consistent with the relative amplitude ratio of u and X in the observational composites (Fig. 11).

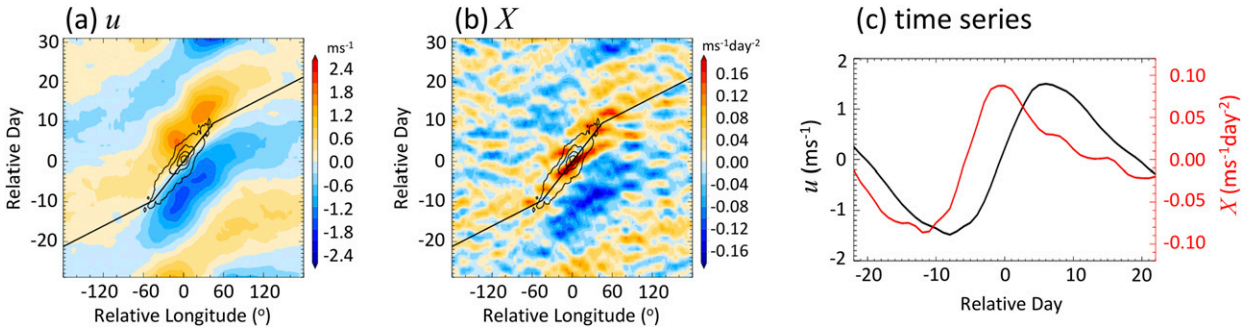

FIG. 11. MJO composites of (a) zonal wind and (b) X in Eq. (5) over 10°S–10°N, 80°–150°E using ERA-Interim overlaid with TRMM precipitation (black contours). Zonal phase speeds are marked by straight black lines, corresponding to 6 m s^{-1} between relative longitudes of −60° and 60°, and 15 m s^{-1} to the west and east. (c) Time series of u (black) and X (red) calculated from (a) and (b). The composite values are averaged between relative longitudes −20° and +20° with a 5-day running average applied.

These matches between the theoretical and observational results suggest the presence of damping in the atmosphere.

b. Feedback

From the first conceptual model of the MJO by Madden and Julian (1972) to date, the MJO is commonly perceived as a consequence of interaction between its dynamics (wind) and convection. Other interaction or feedback processes (cloud radiation, moisture, air–sea interaction) have been proposed for the MJO (see summaries in Jiang et al. 2020; Wang et al. 2016; Zhang et al. 2020). A natural question here would be, based on the simple mathematical framework used in this study, can the MJO exist because of such interaction without any external forcing? In this subsection, we explore this possibility by framing the interaction in terms of feedback between ϕ and u without external forcing. For an analytical solution, the simple mathematical framework allows only a highly idealized representation of such feedback. A minimum requirement is to represent interactions of mass (represented by ϕ) with itself and wind u in the mass conservation equation. We assume the mass source/sink in Eq. (3) takes a linear form involving ϕ and u:

$$\frac{\partial \phi}{\partial t} + gH\frac{\partial u}{\partial x} = au + b\phi, \tag{16}$$

where the first term on the right-hand side au may represent wind-related feedback: easterlies ($u < 0$) induced by a low pressure center would bring moisture into the center and encourage deep convection, which tends to deepen the low pressure center ($\partial\phi/\partial t < 0$) when $a > 0$. The second term $b\phi$ may represent a feedback between convection and pressure: a low pressure center ($\phi < 0$) encourages deep convection which in turn would deepen the low pressure center ($\partial\phi/\partial t < 0$) when $b > 0$. Radiative feedback may also contribute to this as anomalous radiative heating by clouds and moisture during convection encourages more rising motions and convection when $b > 0$ (positive feedback).

With these highly idealized representations of feedback, we seek a solution that is different from the resonant harmonic oscillator presented in section 4 but may still be relevant to the MJO without external forcing. In this case, Eq. (5) becomes

$$\frac{\partial^2 u}{\partial t^2} + D\frac{\partial u}{\partial t} + \omega_0^2 u = -a\frac{\partial u}{\partial x} + b\frac{\partial u}{\partial t} + bDu. \tag{17}$$

Assuming a general solution

$$u(x,t) = e^{\alpha t}e^{i(kx-\omega t)} \tag{18}$$

and plugging it into Eq. (17), we get the growth/decay rate

$$\alpha = \frac{1}{2}\left(a\frac{k}{\omega} + b - D\right) \tag{19}$$

and a dispersion relationship

$$\omega^2 = \frac{1}{8}\left\{4gHk^2 - (b+D)^2 + \sqrt{[4gHk^2 - (b+D)^2]^2 + 16a^2k^2}\right\}. \tag{20}$$

Without feedback ($a = 0$, $b = 0$), the solution becomes the classical simple harmonic oscillation or Kelvin waves ($\alpha = 0$, $\omega = \omega_0$) when $D = 0$ (center in Fig. 12a); when $D \neq 0$ the solution is the standard damped transient harmonic oscillation ($\alpha = -D/2$, $\omega = \omega_D$) (center in Fig. 12b).

With feedback ($a \neq 0$, $b \neq 0$) and damping ($D \neq 0$), an intraseasonal oscillation may exist but only for a small range of the feedback strength a and b (Fig. 12b). This small range is the area above the thick solid white line ($\alpha = 0$), where the amplitude would not decay ($\alpha \geq 0$) and the period is intraseasonal (30–60 days, blue to orange in the background color). Only positive a and b support this intraseasonal oscillation. When a and b are negative, the oscillation can neither grow nor be sustained ($\alpha < 0$). The area corresponding to weak negative α values ($\sim -0.1 < \alpha < 0$) may allow a decaying intraseasonal oscillation similar to the damped solution shown in Fig. 4, but this is only possible when a planetary-scale perturbation already exists.

We compare the left- and right-hand sides of Eq. (17) by calculating their terms from the MJO composite of u from observations. The sum of the left-hand side of Eq. (17) is shown

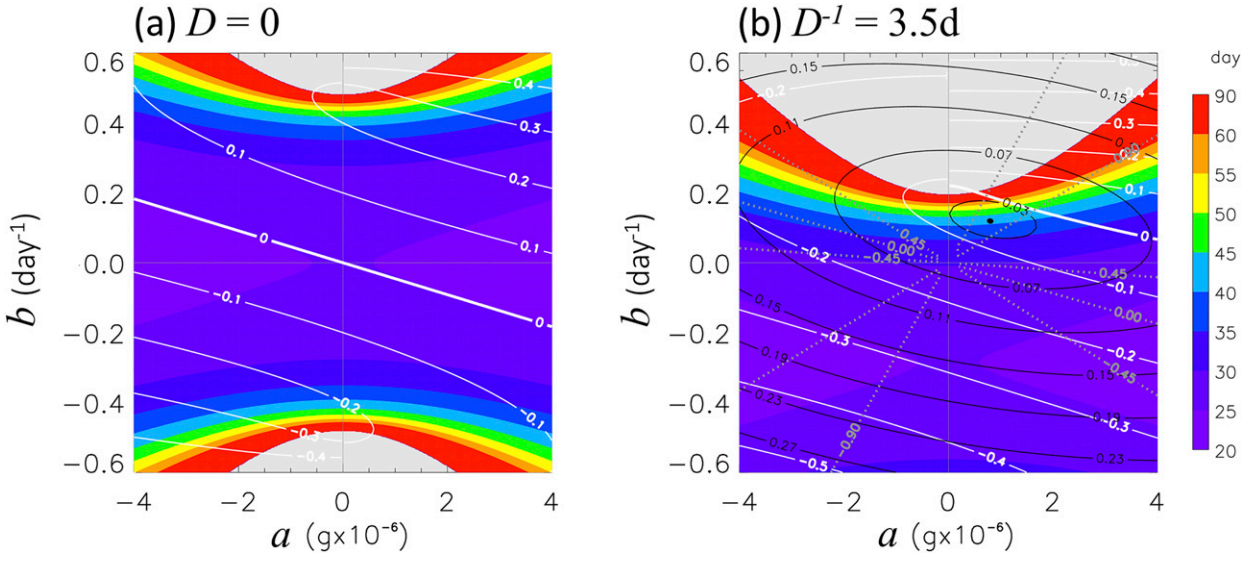

FIG. 12. Periods (color) and the growth/decay rate α (white curves; unit: day^{-1}) as functions of the feedback coefficients a and b based on Eqs. (19) and (20) for (a) $D = 0$ and (b) $D^{-1} = 3.5$ days. Gray area represents either periods > 90 days or no solution. In (b), black lines show the root-mean-square difference (RMSD) between the left-hand side, $\partial^2 u/\partial t^2 + D\partial u/\partial t + \omega_0^2 u$, and the right-hand side, $-a(\partial u/\partial x) + b(\partial u/\partial t) + bDu$, in Eq. (17) using the observed MJO composite of u. Gray dotted lines are correlation coefficients between the two estimates of the left- and right-hand sides in Eq. (17). The black dot corresponds to $a = 0.8$, $b = 0.12$, $\alpha = -0.05$, and a period of 42 days, where the RMSD reaches its minimum and the correlation coefficient its maximum. ω_0 is calculated for $k = 1$ and $H = 35$ m.

in Fig. 11b and the right-hand side is estimated for different values of a and b. This calculation allows us to find feedback strength a and b that are consistent with observations if feedback is present without any other external forcing. The black contours in Fig. 12b show the root-mean-square difference (RMSD) between the left- and right-hand sides of Eq. (17) for given pairs of a and b. The gray dotted lines are correlation coefficients of the left- and right-hand sides of Eq. (17). The calculations are performed near the convection center of the MJO composite within ±30° in longitude and ±20 days in Fig. 11b. The RMSD reaches its minimum at $a = 0.8$ (unit of $g \times 10^{-6}$) and $b = 0.12$ day^{-1} (black point in Fig. 12b) resulting in $\alpha = -0.05$ day^{-1} and period of 42 days. The highest correlation coefficient (>0.9) is also found at this minimum RMSD point. The period of 42 days is consistent with the observed periods of the MJO. RSMD grows away from the minimum RMSD point. This provides an observational constraint for the strength of the feedbacks. While it is straightforward to estimate the period of the MJO from observations, the growth/decay rate α has not been well observed and understood. The negative α at the minimum RMSD point suggests that the MJO may not be a consequence of perturbation growth from feedback alone without external forcing when atmospheric damping–decay effects exceed feedback-growth effects. Although the MJO in the real atmosphere does not seem to be an unstable mode in Fig. 12b, it is possible to simulate intraseasonal instability waves in models if damping is relatively weaker than the feedback strength (e.g., area of positive α and blue to orange background colors for $b > \sim 0.4$ day^{-1} when $D = 0$ in Fig. 12a).

The narrow range in the parameter space of a and b that corresponds to the condition for an intraseasonal oscillation constrained by observations suggests that even when feedback mechanisms are present, such oscillations do not exist all the time. It is allowed only by a right combination of different feedbacks. This result suggests that oscillation characteristics are very sensitive to feedback mechanisms and their magnitudes, and in consequence MJO events energized or sustained solely by feedback processes might be rare. An optimal combination of different feedback effects can help an existing MJO event excited by external forcing persist longer.

The highly idealized representation of the feedback processes nonetheless, this analytical result leads to information applicable to the study of the MJO. If a model cannot simulate the MJO because of its lack of accurate representation of external forcing or feedback processes, it may be tuned to produce an MJO, which is equivalent to move the idealized parameters a and b into the optimal range in Fig. 12. The optimal range depends on the equivalent depth and damping. However, such tuning may be unphysical even when a desirable intraseasonal oscillation is produced, if their corresponding a and b are not constrained as they should. The nonunique combination of a and b needed for feedback processes to be effective to the intraseasonal oscillation may explain the inconsistency between results from several mechanism denial experiments focusing on different feedback mechanisms. Some studies have found that surface-flux feedback is noneffective (Hendon 2000; Sperber et al. 2005), important (DeMott et al. 2014; Maloney and Sobel 2004) or critical (Shi et al. 2018) to the intraseasonal oscillation.

Other studies found radiative feedback can be insignificant (Grabowski 2003) or critical (Andersen and Kuang 2012; Kim et al. 2011) to the MJO. Figure 12 suggests that these discrepancies can be understood as consequences of different combinations of feedback effects with different damping strength.

6. Discussion

Several issues pertaining to the core dynamics of the MJO proposed in sections 5 and 6 deserve more discussions. This core dynamics of the MJO hinges upon zonal momentum damping. The absence of the Rossby waves from this dynamical view on the MJO is inconsistent with some other MJO theories, which needs explanations. A more general comparison between the core dynamics of the MJO and other MJO theories is necessary.

a. Damping scale

In our theory of the MJO core dynamics, the momentum damping plays an essential role in distinguishing the MJO ($k = 1$) from Kelvin waves ($k \geq 2$) in their frequencies, zonal and meridional structures, and phase relationships between zonal wind and geopotential. Several issues related to this essential role of momentum damping in our theoretical explanation for the MJO need to be addressed: Is the value of the damping scale used in this study reasonable? Is linear damping (or Rayleigh damping) a justifiable form to represent momentum damping in the tropical atmosphere? How should the damping scale (or damping coefficient) be estimated? These issues have been discussed in previous studies to certain extents. Here we wish to add our thoughts.

In the lower troposphere, the linear damping term, Du, also known as Rayleigh damping, is generally believed to come mainly from vertical eddy momentum transfer by moist convective processes in addition to a small contribution from advection (Lin et al. 2005) and maybe other processes. Based on theoretical foundations (Moncrieff 1992), possible role of convective momentum transport (CMT) on the large-scale circulation has been demonstrated through parameterization of mesoscale convective systems in global models (Moncrieff 2019; Moncrieff et al. 2017). It is unclear whether CMT is the dominant contribution to the missing part of the momentum budget. In many studies, the momentum damping plays an important role in the atmospheric large-scale circulation and convective evolution. For example, studies have found that a damping scale of 1–10 days is necessary to reproduce observed tropical circulations such as the Walker and monsoon circulations (Gill 1980; Romps 2014). Such values of linear damping have been used in many simple and complex models for tropical atmospheric dynamics, including the MJO (Table 1).

Accurately estimating the value of momentum damping from observations remains an unmet challenge. A common practice of estimating momentum damping is to treat it as a residual of the momentum equation (Lin et al. 2005). Similar to this approach, we calculated $-(\partial u/\partial t + \partial \phi/\partial x)$ at 850 hPa for MJO composites using the reanalysis data, and regressed its value onto u to estimate the damping coefficient D (section 3). Highly simplified nonetheless, this mathematical framework leads to results that suggest that the damping is linearly proportional to zonal wind for the MJO (Fig. 13) and the damping time scale used in this study is consistent with other studies in Table 1.

In MJO composites shown in Fig. 13 zonal wind u in the left panels and the residual of Eq. (1) in the right panels are in phase. If we use the residual as Du to estimate D for individual MJO events within each 10° longitude bins between 80° and 150°E, we can calculate an occurrence frequency distribution of D (Fig. 14). For each MJO event at each longitude bin, $-(\partial u/\partial t + \partial \phi/\partial x) = Du$ can be regressed upon zonal wind u. Data points from relative longitudes between −30° and +30° and relative lag time between −20 and +20 days were used in the regression. The table in Fig. 14 shows the peak, mean, median, and 10th and 90th percentiles of D. The estimated D are not very sensitive to the choice of a regression range for the budget residual and zonal wind. The composite value of 3.7 days was calculated from composites of u and $-(\partial u/\partial t + \partial \phi/\partial x)$ for all MJO events. Estimates of D^{-1} from individual events resulted in the mean and median values of 3.2 and 3.3 days, respectively. All these values are very close to $D^{-1} = 3.5$ days that has been used in many figures of this study.

In topology, the MJO can be considered the lowest mode of topological edge waves in a non-Hermitian (nonconserving) system. Deformation of the wave dispersion is observed in other nonconserving systems such as photonic crystal slabs (Zhen et al. 2015). In this study, we show that equatorial waves also experience a dramatic change in their dispersion due to dissipation (momentum damping). Another interesting issue is the range of the atmospheric damping time scales that brings significant modifications in the lowest mode of Kelvin waves. The missing component from the momentum budget analysis indicates strong dissipation of large-scale wave energy. While the missing momentum may be related to convective processes, it is still unclear why the atmosphere has such damping scales.

Among possible mechanisms, CMT may be the main process of momentum damping. Previous studies have found that CMT can be either a source or sink of momentum for the MJO (Biello et al. 2007; Khouider et al. 2012; Majda and Stechmann 2009a; Miyakawa et al. 2012; Oh et al. 2015; Tung and Yanai 2002; Yang et al. 2019). The results from this study suggest that on average, the zonal momentum has a net sink on the MJO scale, but it is not clear to what extent the theoretical and numerical representations of CMT can be simplified into linear damping. There can be more research to explore whether CMT plays an essential role as a momentum sink of the MJO using both idealized mathematical frameworks and complicated numerical models.

b. MJO and Rossby waves

A large-scale steady-state convective heating excites Kelvin and Rossby waves (Gill 1980; Neelin 1988; Webster 1972). A large-scale slowly moving source would also generate a Rossby wave response if the movement is slow enough compared to the Rossby wave response time scale. Waves start to develop

TABLE 1. Examples of Rayleigh damping time scales from previous studies. (CRM: cloud-resolving model; GMS: gross moist stability; WPG: weak pressure gradient approximation; WTG: weak temperature gradient approximation).

D^{-1} (days)	Topics	Reference
5	MJO	Chang (1977)
2–5	MJO	Neelin et al. (1987)
3–5	MJO	Lin et al. (2005)
5	MJO	Biello and Majda (2005)
1	MJO, 2-day waves	Haertel et al. (2008)
5	MJO	Sugiyama (2009)
1	MJO	Sobel and Maloney (2012)
3	MJO	Adames and Kim (2016)
16	MJO, equatorial waves	Stechmann and Hottovy (2017)
1.8	Tropical circulation	Matsuno (1966)
2.5	Tropical circulation	Gill (1980)
≥3	Rossby waves	Chang and Lim (1982)
2	Tropical circulation	Neelin (1988)
1.25	Tropical circulation	Seager (1991)
2	Tropical circulation	Yu and Neelin (1997)
0.5	Tropical circulation	Raymond and Zeng (2000)
10	Tropical circulation	Wu et al. (2000)
4–10	Tropical circulation	Wu et al. (2001)
2, 10	Gill model and WTG	Bretherton and Sobel (2003)
1–10	Walker circulation	Lin et al. (2008)
4, 10	Equatorial waves	Kuang (2008)
10–20	Teleconnection response	Lee et al. (2009)
1, 10	Tropical Pacific	Carr and Bretherton (2001)
2.5	GMS in CRM	Kuang (2011)
1	WPG vs WTG	Romps (2012)
1–10	Large-scale circulation	Romps (2014)

immediately after a diabatic heating perturbation is generated in the tropics, and tropical and midlatitude wave responses are almost fully established within a week (Jin and Hoskins 1995), suggesting the time scale of MJO convection is slow enough to induce Rossby waves. Equatorial Rossby waves are often observed west of an MJO convection center (Adames and Wallace 2015; Hendon and Salby 1994; Kerns and Chen 2014). However, Rossby wave signals are also present in non-MJO large-scale convective events over the tropical Indian Ocean (Ling et al. 2013). The observations of the nearly perpetual existence of the equatorial Rossby waves associated with the MJO alone are insufficient to confirm that the Rossby waves are a critical dynamical component of the MJO. Such observation has nevertheless motivated many to consider Rossby waves essential to the MJO and to build Rossby waves in MJO theories (Adames and Kim 2016; Biello and Majda 2005; Majda and Stechmann 2009b; Wang and Rui 1990).

Weak wave energy scattering in a spectral space (Delplace et al. 2017) may shed lights on this issue. Wave energy may be transferred to neighboring states if frequencies of different waves are similar. The MJO and planetary-scale Rossby waves have similar frequencies, thus the MJO can induce Rossby waves. Scattering to mixed Rossby–gravity waves is prohibited because mixed Rossby–gravity waves are antisymmetric about the equator. The wave interactions are demonstrated by a topological approach (Delplace et al. 2017): low-frequency Kelvin waves can generate westward Rossby waves due to their similar frequencies, whereas higher-frequency Kelvin waves cannot because there is no available scattering channel that matches the frequency of Rossby waves. In short, the Kelvin–Rossby wave couplet observed in the MJO is a fundamentally allowed wave property, while this couplet at higher frequencies is prohibited.

The presence and absence of the Rossby waves in MJO theories are further discussed in the next subsection.

c. *Comparison with other MJO theories*

All MJO theories include equatorial waves of Matsuno (1966). This is not surprising. As discussed in section 2, the unidirectional propagation of the MJO requires zonal asymmetry. In the tropics, the only source of this zonal asymmetry is the direction of Earth's rotation. The zonal asymmetry in equatorial waves are the immediate dynamical consequences of Earth's rotation. But which equatorial waves to include differ among MJO theories. Many of them include both Kelvin and Rossby waves (Adames and Kim 2016; Biello and Majda 2005; Majda and Stechmann 2009b; Thual et al. 2014; Wang and Rui 1990; Wang et al. 2016). Some of them include only the Rossby waves (Hayashi and Itoh 2017; Rostami and Zeitlin 2019; Yano and Tribbia 2017). Some are based only on Kelvin waves (Chang 1977; Fuchs and Raymond 2017; Wang 1988b). One relies on inertial gravity waves (Yang and Ingersoll 2013, 2014). Without the equatorial waves, a unidirectional mean zonal wind together with anomalous responses in wind to convective heating may create the zonal asymmetry. However, such a unidirectional mean zonal wind does not exist in the Indo-Pacific region where the strongest MJO signals are found (Wang 1988a). In the theories that include both Rossby and Kelvin waves, the role of the Rossby waves is to counteract against the Kelvin waves to provide a zonal asymmetry for moisture to develop more to the east of an MJO center than to its west as the main mechanism for the eastward propagation of the MJO. In our solution of the MJO, the needed zonal asymmetry is provided solely by the dynamics of the Kelvin waves; no Rossby wave is needed.

Some MJO theories explicitly rely on moisture variability. Others, including the one presented in this study, do not. The transient wave solution to the damped harmonic oscillator and the stochastic nature of the needed external forcing in our MJO solution in terms of a resonant harmonic oscillator do not require moisture as a prognostic variable, although moist convection may be one of main sources of the external forcing. Moist convection may induce significant damping effects, which is needed in our approach, but such damping does not exclusively exist for the MJO. Also, coupling to moist convection is needed to lower the equivalent depth H, which is needed in our approach, but this is also universal for all convectively coupled equatorial waves (Dias and Kiladis 2014; Kiladis et al. 2009). Moisture feedback may help sustain MJO convection longer as discussed in section 5b. This study demonstrates that the core dynamics of the MJO does not explicitly

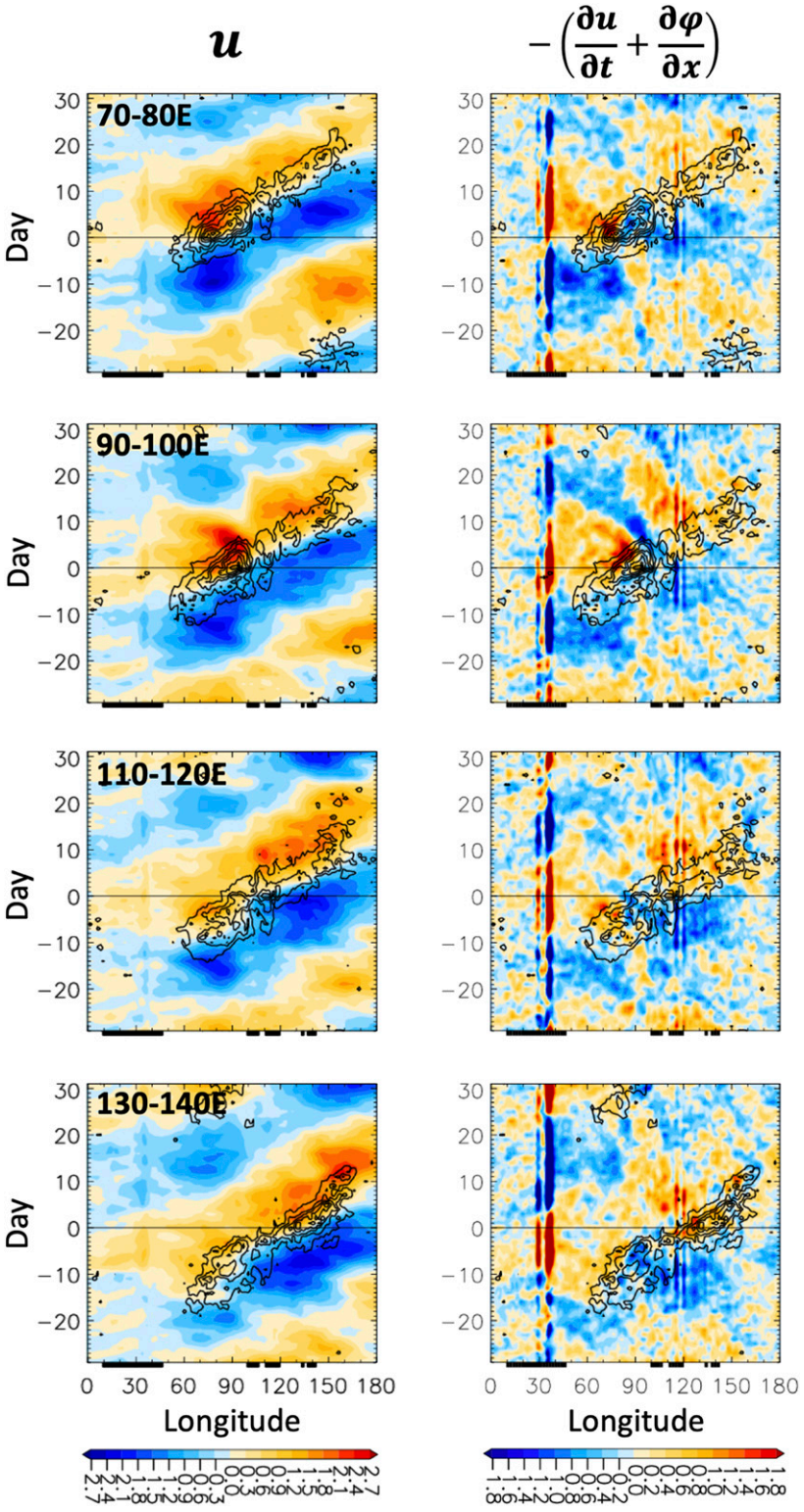

FIG. 13. Longitude–time diagrams of (left) zonal wind u ($\mathrm{m\,s^{-1}}$) and (right) a momentum budget residual $-\partial u/\partial t - \partial\phi/\partial x$ ($\mathrm{m\,s^{-2}}$) as an estimate of Du at 850 hPa from Eq. (1). Data from the ERA-Interim were composited against TRMM precipitation (contours with an interval of 2 mm $\mathrm{day^{-1}}$) for latitudes of 10°S–10°N and longitudes of (from top down) 70°–80°, 90°–100°, 110°–120°, and 130°–140°E during 1998–2014 (see section 3).

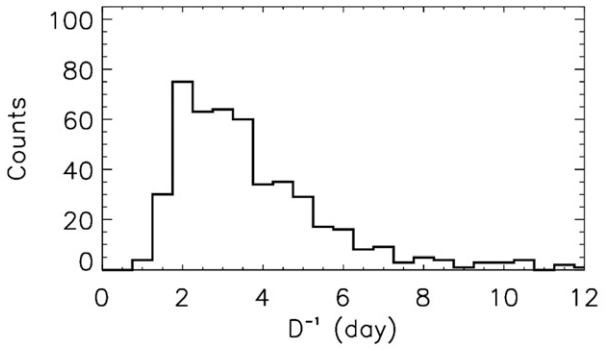

Peak	Mean	Median	From Composite	10th percentile	90th percentile
2.6	3.2	3.3	3.7	1.8	7.2

FIG. 14. Frequency distribution of damping time scales D^{-1} (days) associated with the MJO calculated from zonal wind u and the momentum budget residual $-\partial u/\partial t - \partial\phi/\partial x$ as an estimate of Du over 10°S–10°N, 80°E–150°E using the ERA-Interim data (section 3). The table shows statistical values of damping time scales (days) estimated from the frequency distribution and the composites of u and Du.

depend on moisture variability. The selection of the MJO frequency and zonal scale can comes from damping alone, and the MJO propagates eastward because of exactly the same reason for Kelvin waves to propagate eastward. For these reasons, our perspective on the MJO is analogous to the transition of dry waves to convectively coupled equatorial waves (CCEWs). Although CCEWs require lowering the equivalent depth from the dry wave dynamics, they are not considered as moisture modes. In this case, moisture does not create a new mode of variability, but only changes characteristics of the dry waves. The same principle applies to the MJO core dynamics.

Most MJO theories treat the MJO as an unstable perturbation. An essential part of this classical approach to theoretically explaining the MJO is to explore why the greatest instability or growth rate occurs at the planetary and intraseasonal scales, hence the scale selection of the MJO. The MJO solution as a harmonic oscillator presented in this study is not an unstable perturbation. It is an intrinsic property of the tropical atmosphere that is independent of any external forcing or feedback mechanism, as are the equatorial waves. The MJO solution presented in this study to the observed MJO is as the equatorial wave solutions of Matsuno (1966) to the observed convectively coupled equatorial waves (Kiladis et al. 2009; Wheeler and Kiladis 1999). The only difference is damping is required for the MJO but not for the equatorial waves.

Possible roles of stochastic forcing in the MJO have been explored in different mathematical frameworks (Chen et al. 2014; Deng et al. 2015; Jones 2009). Stochastic forcing may serve as a source of energy for intraseasonal variability (Salby and Garcia 1987; Yu and Neelin 1994), damping for small-scale perturbations as part of the MJO scale selection mechanism (Thual et al. 2014), or a general background for all types of tropical disturbances (Stechmann and Hottovy 2017). In our solution of the MJO, its core dynamics does not depend on stochastic forcing, but stochastic forcing can help energize the MJO.

In the debate of the fundamental dynamics of the MJO, there is no consensus on what is the minimal features of the MJO a theory must explain. To some, an MJO theory should explain as many as possible of all observed features of the MJO, including its three-dimensional, multiscale structures in wind, temperature, moisture, precipitation and other fields, its dependence on the mean background state, its annual and interannual variability, and even its potential trend in a warming climate, as well as its intraseasonal periodicity and eastward propagation. To us, an MJO theory is required to explain only three features of the MJO: its planetary scale, intraseasonal periodicity, and eastward propagation. These three features together are the only ones needed to distinguish the MJO from other tropical perturbations. To readers who disagree, we invite them to do the following exercise: starting from any observed features of the MJO, add others one by one. What would be the minimal number of the features you can name to make an expert on the tropical atmosphere realize that you are talking about the MJO?

Indeed, these three fundamental features alone do not make the observed MJO. An analogy is that a spine alone does not make any living creature a mammal but it is the only feature that distinguishes mammals from other living forms on Earth. The MJO solution presented in this study is a theory of the core dynamics of the MJO (its spine), not the entire MJO.

Because of its simplicity, the MJO solution presented in this study relies on a minimal number of assumptions on the equivalent depth, damping scale, a linear shallow-water system on an equatorial β plane, and a resting mean state. None of them is unique to this MJO solution. In comparison, in other MJO theories, additional assumptions are needed (e.g., on treatment of precipitation, moisture, radiation) to make the MJO unstable preferably at the planetary and intraseasonal scales, and some of these assumptions are unique to a given theory (see examples in Zhang et al. 2020). Based on Occam's razor, the simplicity and the least number of assumptions of the MJO solution presented in this study can be viewed as an advantage of our MJO theory to others.

To revisit the damping scale discussed in section 6a, it should be pointed out that momentum damping is zero in some MJO theories (Fuchs and Raymond 2017; Hayashi and Itoh 2017; Khairoutdinov and Emanuel 2018; Majda and Stechmann 2009b; Yang and Ingersoll 2013, 2014) while it is of similar or greater scales in others (Adames and Kim 2016; Biello and Majda 2005; Wang et al. 2016) in comparison to those used in this study. This discrepancy is merely one of many in the current very diverse thinking and treatment of MJO dynamics (Jiang et al. 2020; Zhang et al. 2020). While the results from the studies with zero damping suggest that the MJO may exist without damping, the real atmosphere is never free of damping. A fair question would be how these results may

change when damping of the commonly used scales (Table 1) is included.

7. Concluding remarks

The pioneering work of Matsuno (1966) predicted equatorially trapped waves in the atmosphere and ocean using linear shallow-water equations on a β plane. Over the years, his analytical solutions have been proven remarkably consistent with observations of tropical disturbances even in the presence of complicated convective feedback processes (Kiladis et al. 2009; Wheeler and Kiladis 1999). The absence of an MJO solution in Matsuno's theory has brought several decades of debate over the fundamental dynamics of the MJO. In this study, we demonstrate that the MJO solution to the Matsuno's equations can be found analytically as a harmonic oscillation by including linear momentum damping.

By no means do we intend to put forth our MJO solution to replace other MJO theories. Our objective is to use the possibly simplest mathematical framework to explain the most fundamental features of the MJO. Once its dynamical core (spine) is present, the MJO would come to life when its other features are added as suggested by other MJO theories. There may not be a single correct MJO theory. Different MJO theories describe their own ways of energizing the core dynamics of the MJO and they all produce the MJO to a certain extent. There are potential energetic sources for the MJO that have yet to be included in MJO theories, for example, energy recharge–discharge (Bladé and Hartmann 1993) and upper-tropospheric perturbations (Powell 2017; Powell and Houze 2015; Sakaeda and Roundy 2016).

It has been suggested that the MJO may propagate faster in a warmer climate (Adames et al. 2017; Maloney et al. 2019; Pritchard and Yang 2016). This can be explained by our theory: In a warmer world, increased static stability would correspond to a greater equivalent depth, which will lead to a great MJO propagation speed. A persistent issue related to the MJO is the prolonged inability of many global models to produce the observed signals of the MJO (Ahn et al. 2017; Jiang et al. 2015; Lin et al. 2006). While we do not think a reasonable MJO theory should be required to explain this, ours may provide some hints. First, the momentum damping required by our MJO solution may not be properly produced by global models. Effects of CMT on the large-scale circulation depend on three-dimensional structures of mesoscale convective systems (Moncrieff 2004), which are not represented by most cumulus parameterization schemes. Second, the effective equivalent depth of the tropical atmosphere may not be in the right range due to biases in static stability or in representation of convective processes through physical parameterizations. Third, models may lack mechanisms to force the tropical atmosphere to resonate at intraseasonal time scales. Last, feedback mechanisms produced by global models may be out of the narrow parameter space that allows an intraseasonal oscillation as illustrated in Fig. 12.

There are many other features of the MJO that the harmonic oscillator solutions do not produce or explain. For example, as other MJO theories, our MJO solution does not explain how MJO events are initiated. It is not our intention to explain everything about the MJO. We seek a possibly simplest approach to explain the most fundamental features of the MJO (its planetary and intraseasonal scales and eastward propagation). The reproduction of the observed swallowtail pattern, poleward propagation, and phase relation between zonal wind and geopotential of the MJO by our solution is a pleasantly surprising bonus.

Every scientific theory must be falsifiable (Popper 1959). The theory of the MJO core dynamics in terms of a harmonic oscillator introduced in this study depends on momentum damping. In section 6a, we demonstrated that the values of linear momentum damping that make our theory viable are within the range of those commonly used in the literature of tropical dynamics, including the MJO. Nonetheless, the mechanism for such momentum damping remains to be identified. Specifically, it is yet to be determined whether CMT can provide the momentum damping needed in our theory. More observational, numerical, and theoretical studies on momentum damping, and convective mass and momentum transport in general would shed lights on the validity of our theory.

Acknowledgments. The authors thank Ángel Adames, Boualem Khouider, Mitch Moncrieff, Paul Roundy, and Sam Stechmann for their valuable comments on an early version of this article. The authors are also grateful to Daehyun Kim, Axel Timmermann, Fei-Fei Jin, Joongoo Kang, and LV Kim for their inspiration and insight during the development of the theory. The work by J.K. was conducted at the Joint Institute for the Study of the Atmosphere and Ocean, University of Washington, while affiliated with the University of Miami supported by an NSF Grant AGS-1450582, and at the Institute for Basic Science (IBS) Center for Climate Physics, Republic of Korea supported by IBS-R028-D1. C.Z. was supported by a NOAA Grant NA13OAR4310161 and by NOAA/PMEL (Contribution Number 4993).

Data availability statement. ERA-Interim data are available from https://www.ecmwf.int. TRMM 3B42 data are available from https://pmm.nasa.gov. The OLR MJO index (OMI) is available from https://www.esrl.noaa.gov/psd/mjo.

REFERENCES

Adames, Á. F., and J. M. Wallace, 2014: Three-dimensional structure and evolution of the MJO and its relation to the mean flow. *J. Atmos. Sci.*, **71**, 2007–2026, https://doi.org/10.1175/JAS-D-13-0254.1.

——, and ——, 2015: Three-dimensional structure and evolution of the moisture field in the MJO. *J. Atmos. Sci.*, **72**, 3733–3754, https://doi.org/10.1175/JAS-D-15-0003.1.

——, and D. Kim, 2016: The MJO as a dispersive, convectively coupled moisture wave: Theory and observations. *J. Atmos. Sci.*, **73**, 913–941, https://doi.org/10.1175/JAS-D-15-0170.1.

——, ——, A. H. Sobel, A. Del Genio, and J. Wu, 2017: Characterization of moist processes associated with changes in the propagation of the MJO with increasing CO_2. *J. Adv. Model. Earth Syst.*, **9**, 2946–2967, https://doi.org/10.1002/2017MS001040.

Ahn, M.-S., and Coauthors, 2017: MJO simulation in CMIP5 climate models: MJO skill metrics and process-oriented diagnosis. *Climate Dyn.*, **49**, 4023–4045, https://doi.org/10.1007/s00382-017-3558-4.

——, and Coauthors, 2020: MJO propagation across the Maritime Continent: Are CMIP6 models better than CMIP5 models? *Geophys. Res. Lett.*, **47**, e2020GL087250, https://doi.org/10.1029/2020GL087250.

Andersen, J. A., and Z. Kuang, 2012: Moist static energy budget of MJO-like disturbances in the atmosphere of a zonally symmetric aquaplanet. *J. Climate*, **25**, 2782–2804, https://doi.org/10.1175/JCLI-D-11-00168.1.

Benedict, J. J., and D. A. Randall, 2007: Observed characteristics of the MJO relative to maximum rainfall. *J. Atmos. Sci.*, **64**, 2332–2354, https://doi.org/10.1175/JAS3968.1.

Biello, J. A., and A. J. Majda, 2005: A new multiscale model for the Madden–Julian oscillation. *J. Atmos. Sci.*, **62**, 1694–1721, https://doi.org/10.1175/JAS3455.1.

——, ——, and M. W. Moncrieff, 2007: Meridional momentum flux and superrotation in the multiscale IPESD MJO model. *J. Atmos. Sci.*, **64**, 1636–1651, https://doi.org/10.1175/JAS3908.1.

Bladé, I., and D. L. Hartmann, 1993: Tropical intraseasonal oscillations in a simple nonlinear model. *J. Atmos. Sci.*, **50**, 2922–2939, https://doi.org/10.1175/1520-0469(1993)050<2922:TIOIAS>2.0.CO;2.

Bretherton, C. S., and A. H. Sobel, 2003: The Gill model and the weak temperature gradient approximation. *J. Atmos. Sci.*, **60**, 451–460, https://doi.org/10.1175/1520-0469(2003)060<0451:TGMATW>2.0.CO;2.

——, M. E. Peters, and L. E. Back, 2004: Relationships between water vapor path and precipitation over the tropical oceans. *J. Climate*, **17**, 1517–1528, https://doi.org/10.1175/1520-0442(2004)017<1517:RBWVPA>2.0.CO;2.

Carr, M. T., and C. S. Bretherton, 2001: Convective momentum transport over the tropical Pacific: Budget estimates. *J. Atmos. Sci.*, **58**, 1673–1693, https://doi.org/10.1175/1520-0469(2001)058<1673:CMTOTT>2.0.CO;2.

Chang, C.-P., 1977: Viscous internal gravity waves and low-frequency oscillations in the tropics. *J. Atmos. Sci.*, **34**, 901–910, https://doi.org/10.1175/1520-0469(1977)034<0901:VIGWAL>2.0.CO;2.

——, and H. Lim, 1982: On the effects of viscous damping on equatorial Rossby waves. *J. Atmos. Sci.*, **39**, 1726–1733, https://doi.org/10.1175/1520-0469(1982)039<1726:OTEOVD>2.0.CO;2.

Chen, N., A. J. Majda, and D. Giannakis, 2014: Predicting the cloud patterns of the Madden-Julian oscillation through a low-order nonlinear stochastic model. *Geophys. Res. Lett.*, **41**, 5612–5619, https://doi.org/10.1002/2014GL060876.

Dee, D. P., and Coauthors, 2011: The ERA-Interim reanalysis: Configuration and performance of the data assimilation system. *Quart. J. Roy. Meteor. Soc.*, **137**, 553–597, https://doi.org/10.1002/qj.828.

Delplace, P., J. B. Marston, and A. Venaille, 2017: Topological origin of equatorial waves. *Science*, **358**, 1075–1077, https://doi.org/10.1126/science.aan8819.

DeMott, C. A., C. Stan, D. A. Randall, and M. D. Branson, 2014: Intraseasonal variability in coupled GCMs: The roles of ocean feedbacks and model physics. *J. Climate*, **27**, 4970–4995, https://doi.org/10.1175/JCLI-D-13-00760.1.

Deng, Q., B. Khouider, and A. J. Majda, 2015: The MJO in a coarse-resolution GCM with a stochastic multicloud parameterization. *J. Atmos. Sci.*, **72**, 55–74, https://doi.org/10.1175/JAS-D-14-0120.1.

Dias, J., and G. N. Kiladis, 2014: Influence of the basic state zonal flow on convectively coupled equatorial waves. *Geophys. Res. Lett.*, **41**, 6904–6913, https://doi.org/10.1002/2014GL061476.

Frederiksen, J. S., and H. Lin, 2013: Tropical–extratropical interactions of intraseasonal oscillations. *J. Atmos. Sci.*, **70**, 3180–3197, https://doi.org/10.1175/JAS-D-12-0302.1.

Fuchs, Ž., and D. J. Raymond, 2017: A simple model of intraseasonal oscillations. *J. Adv. Model. Earth Syst.*, **9**, 1195–1211, https://doi.org/10.1002/2017MS000963.

Gill, A. E., 1980: Some simple solutions for heat-induced tropical circulation. *Quart. J. Roy. Meteor. Soc.*, **106**, 447–462, https://doi.org/10.1002/qj.49710644905.

Gottschalck, J., P. E. Roundy, C. J. Schreck III, A. Vintzileos, and C. Zhang, 2013: Large-scale atmospheric and oceanic conditions during the 2011–12 DYNAMO field campaign. *Mon. Wea. Rev.*, **141**, 4173–4196, https://doi.org/10.1175/MWR-D-13-00022.1.

Grabowski, W. W., 2003: MJO-like coherent structures: Sensitivity simulations using the cloud-resolving convection parameterization (CRCP). *J. Atmos. Sci.*, **60**, 847–864, https://doi.org/10.1175/1520-0469(2003)060<0847:MLCSSS>2.0.CO;2.

Haertel, P. T., G. N. Kiladis, A. Denno, and T. M. Rickenbach, 2008: Vertical-mode decompositions of 2-day waves and the Madden–Julian oscillation. *J. Atmos. Sci.*, **65**, 813–833, https://doi.org/10.1175/2007JAS2314.1.

Hashemi, M., 2016: Analytical and numerical studies of thalamocortical neural population models during general anesthesia. Thèse doctorat, Université de Lorraine, 199 pp., https://hal.inria.fr/tel-01754610v2/document.

Hayashi, M., and H. Itoh, 2017: A new mechanism of the slow eastward propagation of unstable disturbances with convection in the tropics: Implications for the MJO. *J. Atmos. Sci.*, **74**, 3749–3769, https://doi.org/10.1175/JAS-D-16-0300.1.

Hendon, H. H., 2000: Impact of air–sea coupling on the Madden–Julian oscillation in a general circulation model. *J. Atmos. Sci.*, **57**, 3939–3952, https://doi.org/10.1175/1520-0469(2001)058<3939:IOASCO>2.0.CO;2.

——, and M. L. Salby, 1994: The life cycle of the Madden–Julian oscillation. *J. Atmos. Sci.*, **51**, 2225–2237, https://doi.org/10.1175/1520-0469(1994)051<2225:TLCOTM>2.0.CO;2.

Hsu, H.-H., B. J. Hoskins, and F.-F. Jin, 1990: The 1985/86 intraseasonal oscillation and the role of the extratropics. *J. Atmos. Sci.*, **47**, 823–839, https://doi.org/10.1175/1520-0469(1990)047<0823:TIOATR>2.0.CO;2.

Huffman, G. J., and Coauthors, 2007: The TRMM Multisatellite Precipitation Analysis (TMPA): Quasi-global, multiyear, combined-sensor precipitation estimates at fine scales. *J. Hydrometeor.*, **8**, 38–55, https://doi.org/10.1175/JHM560.1.

Jiang, X., T. Li, and B. Wang, 2004: Structures and mechanisms of the northward propagating boreal summer intraseasonal oscillation. *J. Climate*, **17**, 1022–1039, https://doi.org/10.1175/1520-0442(2004)017<1022:SAMOTN>2.0.CO;2.

——, and Coauthors, 2015: Vertical structure and physical processes of the Madden-Julian oscillation: Exploring key model physics in climate simulations. *J. Geophys. Res. Atmos.*, **120**, 4718–4748, https://doi.org/10.1002/2014JD022375.

——, and Coauthors, 2020: Fifty years of research on the Madden-Julian oscillation: Recent progress, challenges, and perspectives. *J. Geophys. Res. Atmos.*, **125**, e2019JD030911, https://doi.org/10.1029/2019JD030911.

Jin, F., and B. J. Hoskins, 1995: The direct response to tropical heating in a baroclinic atmosphere. *J. Atmos. Sci.*, **52**, 307–319,

https://doi.org/10.1175/1520-0469(1995)052<0307:TDRTTH>2.0.CO;2.

Johnson, R. H., P. E. Ciesielski, J. H. R. Jr, and M. Katsumata, 2015: Sounding-based thermodynamic budgets for DYNAMO. *J. Atmos. Sci.*, **72**, 598–622, https://doi.org/10.1175/JAS-D-14-0202.1.

Jones, C., 2009: A homogeneous stochastic model of the Madden–Julian oscillation. *J. Climate*, **22**, 3270–3288, https://doi.org/10.1175/2008JCLI2609.1.

Kemball-Cook, S., and B. Wang, 2001: Equatorial waves and air–sea interaction in the boreal summer intraseasonal oscillation. *J. Climate*, **14**, 2923–2942, https://doi.org/10.1175/1520-0442(2001)014<2923:EWAASI>2.0.CO;2.

——, and B. C. Weare, 2001: The onset of convection in the Madden–Julian oscillation. *J. Climate*, **14**, 780–793, https://doi.org/10.1175/1520-0442(2001)014<0780:TOOCIT>2.0.CO;2.

Kerns, B. W., and S. S. Chen, 2014: Equatorial dry air intrusion and related synoptic variability in MJO initiation during DYNAMO. *Mon. Wea. Rev.*, **142**, 1326–1343, https://doi.org/10.1175/MWR-D-13-00159.1.

Khairoutdinov, M. F., and K. Emanuel, 2018: Intraseasonal variability in a cloud-permitting near-global equatorial aquaplanet model. *J. Atmos. Sci.*, **75**, 4337–4355, https://doi.org/10.1175/JAS-D-18-0152.1.

Khouider, B., Y. Han, A. J. Majda, and S. N. Stechmann, 2012: Multiscale waves in an MJO background and convective momentum transport feedback. *J. Atmos. Sci.*, **69**, 915–933, https://doi.org/10.1175/JAS-D-11-0152.1.

Kikuchi, K., and Y. N. Takayabu, 2004: The development of organized convection associated with the MJO during TOGA COARE IOP: Trimodal characteristics. *Geophys. Res. Lett.*, **31**, L10101, https://doi.org/10.1029/2004GL019601.

Kiladis, G. N., K. H. Straub, and P. T. Haertel, 2005: Zonal and vertical structure of the Madden–Julian oscillation. *J. Atmos. Sci.*, **62**, 2790–2809, https://doi.org/10.1175/JAS3520.1.

——, M. C. Wheeler, P. T. Haertel, K. H. Straub, and P. E. Roundy, 2009: Convectively coupled equatorial waves. *Rev. Geophys.*, **47**, RG2003, https://doi.org/10.1029/2008RG000266.

——, and Coauthors, 2014: A comparison of OLR and circulation-based indices for tracking the MJO. *Mon. Wea. Rev.*, **142**, 1697–1715, https://doi.org/10.1175/MWR-D-13-00301.1.

Kim, D., A. H. Sobel, and I.-S. Kang, 2011: A mechanism denial study on the Madden-Julian oscillation. *J. Adv. Model. Earth Syst.*, **3**, M12007, https://doi.org/10.1029/2011MS000081.

Kuang, Z., 2008: Modeling the interaction between cumulus convection and linear gravity waves using a limited-domain cloud system–resolving model. *J. Atmos. Sci.*, **65**, 576–591, https://doi.org/10.1175/2007JAS2399.1.

——, 2011: The wavelength dependence of the gross moist stability and the scale selection in the instability of column-integrated moist static energy. *J. Atmos. Sci.*, **68**, 61–74, https://doi.org/10.1175/2010JAS3591.1.

Lau, K.-M., and L. Peng, 1987: Origin of low-frequency (intraseasonal) oscillations in the tropical atmosphere. Part I: Basic theory. *J. Atmos. Sci.*, **44**, 950–972, https://doi.org/10.1175/1520-0469(1987)044<0950:OOLFOI>2.0.CO;2.

——, P.-J. Sheu, and I.-S. Kang, 1994: Multiscale low-frequency circulation modes in the global atmosphere. *J. Atmos. Sci.*, **51**, 1169–1193, https://doi.org/10.1175/1520-0469(1994)051<1169:MLFCMI>2.0.CO;2.

Lee, S.-K., C. Wang, and B. E. Mapes, 2009: A simple atmospheric model of the local and teleconnection responses to tropical heating anomalies. *J. Climate*, **22**, 272–284, https://doi.org/10.1175/2008JCLI2303.1.

Lin, J.-L., M. Zhang, and B. Mapes, 2005: Zonal momentum budget of the Madden–Julian oscillation: The source and strength of equivalent linear damping. *J. Atmos. Sci.*, **62**, 2172–2188, https://doi.org/10.1175/JAS3471.1.

——, and Coauthors, 2006: Tropical intraseasonal variability in 14 IPCC AR4 climate models. Part I: Convective signals. *J. Climate*, **19**, 2665–2690, https://doi.org/10.1175/JCLI3735.1.

——, B. E. Mapes, and W. Han, 2008: What are the sources of mechanical damping in Matsuno–Gill-type models? *J. Climate*, **21**, 165–179, https://doi.org/10.1175/2007JCLI1546.1.

Lin, X., and R. H. Johnson, 1996: Heating, moistening, and rainfall over the western Pacific warm pool during TOGA COARE. *J. Atmos. Sci.*, **53**, 3367–3383, https://doi.org/10.1175/1520-0469(1996)053<3367:HMAROT>2.0.CO;2.

Ling, J., C. Zhang, and P. Bechtold, 2013: Large-scale distinctions between MJO and non-MJO convective initiation over the tropical Indian Ocean. *J. Atmos. Sci.*, **70**, 2696–2712, https://doi.org/10.1175/JAS-D-13-029.1.

Madden, R. A., and P. R. Julian, 1971: Detection of a 40–50 day oscillation in the zonal wind in the tropical Pacific. *J. Atmos. Sci.*, **28**, 702–708, https://doi.org/10.1175/1520-0469(1971)028<0702:DOADOI>2.0.CO;2.

——, and ——, 1972: Description of global-scale circulation cells in the tropics with a 40–50 day period. *J. Atmos. Sci.*, **29**, 1109–1123, https://doi.org/10.1175/1520-0469(1972)029<1109:DOGSCC>2.0.CO;2.

Majda, A. J., and S. N. Stechmann, 2009a: A simple dynamical model with features of convective momentum transport. *J. Atmos. Sci.*, **66**, 373–392, https://doi.org/10.1175/2008JAS2805.1.

——, and ——, 2009b: The skeleton of tropical intraseasonal oscillations. *Proc. Natl. Acad. Sci. USA*, **106**, 8417–8422, https://doi.org/10.1073/pnas.0903367106.

Maloney, E. D., and A. H. Sobel, 2004: Surface fluxes and ocean coupling in the tropical intraseasonal oscillation. *J. Climate*, **17**, 4368–4386, https://doi.org/10.1175/JCLI-3212.1.

——, Á. F. Adames, and H. X. Bui, 2019: Madden–Julian oscillation changes under anthropogenic warming. *Nat. Climate Change*, **9**, 26–33, https://doi.org/10.1038/s41558-018-0331-6.

Masoliver, J., and J. M. Porrà, 1993: Harmonic oscillators driven by colored noise: Crossovers, resonances, and spectra. *Phys. Rev.*, **48E**, 4309–4319, https://doi.org/10.1103/PhysRevE.48.4309.

Matsuno, T., 1966: Quasi-geostrophic motions in the equatorial area. *J. Meteor. Soc. Japan*, **44**, 25–43, https://doi.org/10.2151/jmsj1965.44.1_25.

Matthews, A. J., 2008: Primary and successive events in the Madden–Julian oscillation. *Quart. J. Roy. Meteor. Soc.*, **134**, 439–453, https://doi.org/10.1002/qj.224.

——, B. J. Hoskins, J. M. Slingo, and M. Blackburn, 1996: Development of convection along the SPCZ within a Madden-Julian oscillation. *Quart. J. Roy. Meteor. Soc.*, **122**, 669–688, https://doi.org/10.1002/qj.49712253106.

Meehl, G. A., C. Shields, J. M. Arblaster, H. Annamalai, and R. Neale, 2020: Intraseasonal, seasonal, and interannual characteristics of regional monsoon simulations in CESM2. *J. Adv. Model. Earth Sys.*, **12**, e2019MS001962, https://doi.org/10.1029/2019MS001962.

Miyakawa, T., Y. N. Takayabu, T. Nasuno, H. Miura, M. Satoh, and M. W. Moncrieff, 2012: Convective momentum transport by rainbands within a Madden–Julian oscillation in a global nonhydrostatic model with explicit deep convective processes.

Part I: Methodology and general results. *J. Atmos. Sci.*, **69**, 1317–1338, https://doi.org/10.1175/JAS-D-11-024.1.

Moncrieff, M. W., 1992: Organized convective systems: Archetypal dynamical models, mass and momentum flux theory, and parametrization. *Quart. J. Roy. Meteor. Soc.*, **118**, 819–850, https://doi.org/10.1002/qj.49711850703.

——, 2004: Analytic representation of the large-scale organization of tropical convection. *J. Atmos. Sci.*, **61**, 1521–1538, https://doi.org/10.1175/1520-0469(2004)061<1521:AROTLO>2.0.CO;2.

——, 2019: Toward a dynamical foundation for organized convection parameterization in GCMs. *Geophys. Res. Lett.*, **46**, 14 103–14 108, https://doi.org/10.1029/2019GL085316.

——, C. Liu, and P. Bogenschutz, 2017: Simulation, modeling, and dynamically based parameterization of organized tropical convection for global climate models. *J. Atmos. Sci.*, **74**, 1363–1380, https://doi.org/10.1175/JAS-D-16-0166.1.

Moore, J. E., 2010: The birth of topological insulators. *Nature*, **464**, 194–198, https://doi.org/10.1038/nature08916.

Myers, D. S., and D. E. Waliser, 2003: Three-dimensional water vapor and cloud variations associated with the Madden–Julian oscillation during Northern Hemisphere winter. *J. Climate*, **16**, 929–950, https://doi.org/10.1175/1520-0442(2003)016<0929:TDWVAC>2.0.CO;2.

National Academies of Sciences, Engineering, and Medicine, 2016: *Next Generation Earth System Prediction: Strategies for Subseasonal to Seasonal Forecasts.* National Academies Press, 350 pp.

Neelin, J. D., 1988: A simple model for surface stress and low-level flow in the tropical atmosphere driven by prescribed heating. *Quart. J. Roy. Meteor. Soc.*, **114**, 747–770, https://doi.org/10.1002/qj.49711448110.

——, I. M. Held, and K. H. Cook, 1987: Evaporation-wind feedback and low-frequency variability in the tropical atmosphere. *J. Atmos. Sci.*, **44**, 2341–2348, https://doi.org/10.1175/1520-0469(1987)044<2341:EWFALF>2.0.CO;2.

Oh, J.-H., X. Jiang, D. E. Waliser, M. W. Moncrieff, and R. H. Johnson, 2015: Convective momentum transport associated with the Madden–Julian oscillation based on a reanalysis dataset. *J. Climate*, **28**, 5763–5782, https://doi.org/10.1175/JCLI-D-14-00570.1.

Popper, K., 1959: *The Logic of Scientific Discovery*. Routledge, 479 pp.

Powell, S. W., 2017: Successive MJO propagation in MERRA-2 reanalysis. *Geophys. Res. Lett.*, **44**, 5178–5186, https://doi.org/10.1002/2017GL073399.

——, and R. A. Houze Jr., 2015: Effect of dry large-scale vertical motions on initial MJO convective onset. *J. Geophys. Res. Atmos.*, **120**, 4783–4805, https://doi.org/10.1002/2014JD022961.

Pritchard, M. S., and D. Yang, 2016: Response of the superparameterized Madden–Julian oscillation to extreme climate and basic-state variation challenges a moisture mode view. *J. Climate*, **29**, 4995–5008, https://doi.org/10.1175/JCLI-D-15-0790.1.

Qi, Y., R. Zhang, X. Rong, J. Li, and L. Li, 2019: Boreal summer intraseasonal oscillation in the Asian–Pacific monsoon region simulated in CAMS-CSM. *J. Meteor. Res.*, **33**, 66–79, https://doi.org/10.1007/s13351-019-8080-7.

Ray, P., C. Zhang, J. Dudhia, and S. S. Chen, 2009: A numerical case study on the initiation of the Madden–Julian oscillation. *J. Atmos. Sci.*, **66**, 310–331, https://doi.org/10.1175/2008JAS2701.1.

Raymond, D. J., 2001: A new model of the Madden–Julian oscillation. *J. Atmos. Sci.*, **58**, 2807–2819, https://doi.org/10.1175/1520-0469(2001)058<2807:ANMOTM>2.0.CO;2.

——, and X. Zeng, 2000: Instability and large-scale circulations in a two-column model of the tropical troposphere. *Quart. J. Roy. Meteor. Soc.*, **126**, 3117–3135, https://doi.org/10.1002/qj.49712657007.

——, and Ž. Fuchs, 2009: Moisture modes and the Madden–Julian oscillation. *J. Climate*, **22**, 3031–3046, https://doi.org/10.1175/2008JCLI2739.1.

Romps, D. M., 2012: Weak pressure gradient approximation and its analytical solutions. *J. Atmos. Sci.*, **69**, 2835–2845, https://doi.org/10.1175/JAS-D-11-0336.1.

——, 2014: Rayleigh damping in the free troposphere. *J. Atmos. Sci.*, **71**, 553–565, https://doi.org/10.1175/JAS-D-13-062.1.

Rostami, M., and V. Zeitlin, 2019: Eastward-moving convection-enhanced modons in shallow water in the equatorial tangent plane. *Phys. Fluids*, **31**, 021701, https://doi.org/10.1063/1.5080415.

Roundy, P. E., 2012: The spectrum of convectively coupled Kelvin waves and the Madden–Julian oscillation in regions of low-level easterly and westerly background flow. *J. Atmos. Sci.*, **69**, 2107–2111, https://doi.org/10.1175/JAS-D-12-060.1.

——, 2014: Some aspects of western hemisphere circulation and the Madden–Julian oscillation. *J. Atmos. Sci.*, **71**, 2027–2039, https://doi.org/10.1175/JAS-D-13-0210.1.

——, 2019: Interpretation of the spectrum of eastward-moving tropical convective anomalies. *Quart. J. Roy. Meteor. Soc.*, **146**, 795–806, https://doi.org/10.1002/qj.3709.

Sakaeda, N., and P. E. Roundy, 2016: The development of upper-tropospheric geopotential height anomaly in the Western Hemisphere during MJO convective initiations. *Quart. J. Roy. Meteor. Soc.*, **142**, 942–956, https://doi.org/10.1002/qj.2696.

Salby, M. L., and R. R. Garcia, 1987: Transient response to localized episodic heating in the tropics. Part I: Excitation and short-time near-field behavior. *J. Atmos. Sci.*, **44**, 458–498, https://doi.org/10.1175/1520-0469(1987)044<0458:TRTLEH>2.0.CO;2.

Seager, R., 1991: A simple model of the climatology and variability of the low-level wind field in the tropics. *J. Climate*, **4**, 164–179, https://doi.org/10.1175/1520-0442(1991)004<0164:ASMOTC>2.0.CO;2.

Shi, X., D. Kim, Á. F. Adames, and J. Sukhatme, 2018: WISHE-moisture mode in an aquaplanet simulation. *J. Adv. Model. Earth Syst.*, **10**, 2393–2407, https://doi.org/10.1029/2018MS001441.

Sikka, D. R., and S. Gadgil, 1980: On the maximum cloud zone and the ITCZ over Indian longitudes during the southwest monsoon. *Mon. Wea. Rev.*, **108**, 1840–1853, https://doi.org/10.1175/1520-0493(1980)108<1840:OTMCZA>2.0.CO;2.

Sobel, A., and E. Maloney, 2012: An idealized semi-empirical framework for modeling the Madden–Julian oscillation. *J. Atmos. Sci.*, **69**, 1691–1705, https://doi.org/10.1175/JAS-D-11-0118.1.

Son, S.-W., Y. Lim, C. Yoo, H. H. Hendon, and J. Kim, 2017: Stratospheric control of the Madden–Julian oscillation. *J. Climate*, **30**, 1909–1922, https://doi.org/10.1175/JCLI-D-16-0620.1.

Sperber, K. R., S. Gualdi, S. Legutke, and V. Gayler, 2005: The Madden–Julian oscillation in ECHAM4 coupled and uncoupled general circulation models. *Climate Dyn.*, **25**, 117–140, https://doi.org/10.1007/s00382-005-0026-3.

Stechmann, S. N., and S. Hottovy, 2017: Unified spectrum of tropical rainfall and waves in a simple stochastic model. *Geophys. Res. Lett.*, **44**, 10 713–10 724, https://doi.org/10.1002/2017GL075754.

Sugiyama, M., 2009: The moisture mode in the quasi-equilibrium tropical circulation model. Part II: Nonlinear behavior on an

equatorial β plane. *J. Atmos. Sci.*, **66**, 1525–1542, https://doi.org/10.1175/2008JAS2691.1.

Thual, S., A. J. Majda, and S. N. Stechmann, 2014: A stochastic skeleton model for the MJO. *J. Atmos. Sci.*, **71**, 697–715, https://doi.org/10.1175/JAS-D-13-0186.1.

Tung, W.-W., and M. Yanai, 2002: Convective momentum transport observed during the TOGA COARE IOP. Part II: Case studies. *J. Atmos. Sci.*, **59**, 2535–2549, https://doi.org/10.1175/1520-0469(2002)059<2535:CMTODT>2.0.CO;2.

Virts, K. S., and J. M. Wallace, 2014: Observations of temperature, wind, cirrus, and trace gases in the tropical tropopause transition layer during the MJO. *J. Atmos. Sci.*, **71**, 1143–1157, https://doi.org/10.1175/JAS-D-13-0178.1.

Waliser, D. E., K. M. Lau, W. Stern, and C. Jones, 2003: Potential predictability of the Madden–Julian oscillation. *Bull. Amer. Meteor. Soc.*, **84**, 33–50, https://doi.org/10.1175/BAMS-84-1-33.

Wang, B., 1988a: Comments on ''An air–sea interaction model of intraseasonal oscillation in the tropics.'' *J. Atmos. Sci.*, **45**, 3521–3525, https://doi.org/10.1175/1520-0469(1988)045<3521:COAIMO>2.0.CO;2.

——, 1988b: Dynamics of tropical low-frequency waves: An analysis of the moist Kelvin wave. *J. Atmos. Sci.*, **45**, 2051–2065, https://doi.org/10.1175/1520-0469(1988)045<2051:DOTLFW>2.0.CO;2.

——, and H. Rui, 1990: Dynamics of the coupled moist Kelvin–Rossby wave on an equatorial β-plane. *J. Atmos. Sci.*, **47**, 397–413, https://doi.org/10.1175/1520-0469(1990)047<0397:DOTCMK>2.0.CO;2.

——, F. Liu, and G. Chen, 2016: A trio-interaction theory for Madden–Julian oscillation. *Geosci. Lett.*, **3**, 34, https://doi.org/10.1186/s40562-016-0066-z.

Weare, B. C., 2003: Composite singular value decomposition analysis of moisture variations associated with the Madden–Julian oscillation. *J. Climate*, **16**, 3779–3792, https://doi.org/10.1175/1520-0442(2003)016<3779:CSVDAO>2.0.CO;2.

Webster, P. J., 1972: Response of the tropical atmosphere to local, steady forcing. *Mon. Wea. Rev.*, **100**, 518–541, https://doi.org/10.1175/1520-0493(1972)100<0518:ROTTAT>2.3.CO;2.

Wheeler, M., and G. N. Kiladis, 1999: Convectively coupled equatorial waves: Analysis of clouds and temperature in the wavenumber–frequency domain. *J. Atmos. Sci.*, **56**, 374–399, https://doi.org/10.1175/1520-0469(1999)056<0374:CCEWAO>2.0.CO;2.

Wu, Z., D. S. Battisti, and E. S. Sarachik, 2000: Rayleigh friction, Newtonian cooling, and the linear response to steady tropical heating. *J. Atmos. Sci.*, **57**, 1937–1957, https://doi.org/10.1175/1520-0469(2000)057<1937:RFNCAT>2.0.CO;2.

——, E. S. Sarachik, and D. S. Battisti, 2001: Thermally driven tropical circulations under Rayleigh friction and Newtonian cooling: Analytic solutions. *J. Atmos. Sci.*, **58**, 724–741, https://doi.org/10.1175/1520-0469(2001)058<0724:TDTCUR>2.0.CO;2.

Yang, D., and A. P. Ingersoll, 2013: Triggered convection, gravity waves, and the MJO: A shallow-water model. *J. Atmos. Sci.*, **70**, 2476–2486, https://doi.org/10.1175/JAS-D-12-0255.1.

——, and ——, 2014: A theory of the MJO horizontal scale. *Geophys. Res. Lett.*, **41**, 1059–1064, https://doi.org/10.1002/2013GL058542.

Yang, Q., A. J. Majda, and M. W. Moncrieff, 2019: Upscale impact of mesoscale convective systems and its parameterization in an idealized GCM for an MJO analog above the equator. *J. Atmos. Sci.*, **76**, 865–892, https://doi.org/10.1175/JAS-D-18-0260.1.

Yano, J.-I., and J. J. Tribbia, 2017: Tropical atmospheric Madden–Julian oscillation: A strongly nonlinear free solitary Rossby wave? *J. Atmos. Sci.*, **74**, 3473–3489, https://doi.org/10.1175/JAS-D-16-0319.1.

Yasunari, T., 1979: Cloudiness fluctuations associated with the Northern Hemisphere summer monsoon. *J. Meteor. Soc. Japan*, **57**, 227–242, https://doi.org/10.2151/jmsj1965.57.3_227.

——, 1980: A quasi-stationary appearance of 30- to 40-day period in the cloudiness fluctuations during the summer monsoon over India. *J. Meteor. Soc. Japan*, **58**, 225–229, https://doi.org/10.2151/jmsj1965.58.3_225.

Yu, J.-Y., and J. D. Neelin, 1994: Modes of tropical variability under convective adjustment and the Madden–Julian oscillation. Part II: Numerical results. *J. Atmos. Sci.*, **51**, 1895–1914, https://doi.org/10.1175/1520-0469(1994)051<1895:MOTVUC>2.0.CO;2.

——, and ——, 1997: Analytic approximations for moist convectively adjusted regions. *J. Atmos. Sci.*, **54**, 1054–1063, https://doi.org/10.1175/1520-0469(1997)054<1054:AAFMCA>2.0.CO;2.

Zhang, C., 2005: Madden-Julian oscillation. *Rev. Geophys.*, **43**, RG2003, https://doi.org/10.1029/2004RG000158.

——, 2013: Madden–Julian oscillation: Bridging weather and climate. *Bull. Amer. Meteor. Soc.*, **94**, 1849–1870, https://doi.org/10.1175/BAMS-D-12-00026.1.

——, and J. Ling, 2012: Potential vorticity of the Madden–Julian oscillation. *J. Atmos. Sci.*, **69**, 65–78, https://doi.org/10.1175/JAS-D-11-081.1.

——, and ——, 2017: Barrier effect of the Indo-Pacific maritime continent on the MJO: Perspectives from tracking MJO precipitation. *J. Climate*, **30**, 3439–3459, https://doi.org/10.1175/JCLI-D-16-0614.1.

——, Á. F. Adames, B. Khouider, B. Wang, and D. Yang, 2020: Four theories of the Madden-Julian oscillation. *Rev. Geophys.*, **58**, e2019RG000685, https://doi.org/10.1029/2019RG000685.

Zhen, B., and Coauthors, 2015: Spawning rings of exceptional points out of Dirac cones. *Nature*, **525**, 354–358, https://doi.org/10.1038/nature14889.